BMI/OWTD-7
Distribution Category UC-802

BMI/OWTD--7

DE91 000670

Large Block Migration Experiments INTRAVAL Phase I, Test Case 9

Technical Report

August 1990

prepared by

A. Berge Gureghian
Clifford J. Noronha*
of
Office of Waste Technology Development

and

Tjalle T. Vandergraaf
of
Atomic Energy Canada Limited

prepared for

Office of Waste Technology Development
Battelle Energy Systems Group
7000 South Adams Street
Willowbrook, IL 60521

This report was prepared by Battelle Energy Systems Group, Willowbrook, IL, under Contract No. DE-AC02-83CH10139 with the U.S. Department of Energy.

*Presently with Roy F. Weston, Inc.

ABSTRACT

The development of INTRAVAL Test Case 9, as presented in this report, was made possible by a past subsidiary agreement to the bilateral cooperative agreement between the U.S. Department of Energy (DOE) and Atomic Energy of Canada Limited (AECL) encompassing various aspects of nuclear waste disposal research. The experimental aspect of this test case, which included a series of laboratory experiments designed to quantify the migration of tracers in a single, natural fracture, was undertaken by AECL. The numerical simulation of the results of these experiments was performed by the Battelle Office of Waste Technology Development (OWTD) by calibrating an in-house analytical code, FRACFLO, which is capable of predicting radionuclide transport in an idealized fractured rock.

Three tracer migration experiments were performed, using nonsorbing uranine dye for two of them and sorbing Cs-137 for the third. In addition, separate batch experiments were performed to determine the fracture surface and rock matrix sorption coefficients for Cs-137. The two uranine tracer migration experiments were used to calculate the average fracture aperture and to calibrate the model for the fracture dispersivity and matrix diffusion coefficient. The predictive capability of the model was then tested by simulating the third, Cs-137, tracer test without changing the parameter values determined from the other experiments. Breakthrough curves of both the experimental and numerical results obtained at the outlet face of the fracture are presented for each experiment. The reported spatial concentration profiles for the rock matrix are based solely on numerical predictions.

TABLE OF CONTENTS

TABLE OF CONTENTS
(Continued)

LIST OF TABLES

LIST OF FIGURES

LIST OF FIGURES
(Continued)

LIST OF TABLES

LIST OF FIGURES

LIST OF FIGURES
(Continued)

I. INTRODUCTION

Atomic Energy of Canada Limited (AECL) performed the Large Block Experiment, which was designed to understand the processes affecting the migration of tracers in a single fracture. The Battelle Office of Waste Technology Development (OWTD) was responsible for simulating the laboratory results of this experiment using mathematical models of single fracture radionuclide transport. The Test Case 9 definition describes the details of the experimental design results as well as the corresponding simulations using the computer code FRACFLO (Gureghian, 1990).

I-A. PILOT GROUP IDENTIFICATION

The Pilot Group for Test Case 9 is the OWTD located in Willowbrook, Illinois, USA. The Pilot Group Leader is A. Berge Gureghian.

I-B. EXPERIMENT LOCATION

The experiments were carried out in a laboratory at the AECL Whiteshell Nuclear Research Establishment (WNRE) located near Pinawa, Manitoba, Canada. The experiments were carried out in the Geochemistry Section of the Geochemistry and Applied Chemistry Branch by Daniel M. Grondin and Doug J. Drew under the direction of Tjalle T. Vandergraaf.

I C. OBJECTIVES

The objectives of this exercise have been:

- To calibrate mathematical models simulating radionuclide transport in a single planar fracture including matrix diffusion.

- To test the adequacy of the calibrated values, the experimental approach, and applicable mathematical models. For these objectives, data were obtained from tracer migration experiments carried out in a natural fracture in a granite block obtained from a surface quarry near Lac du Bonnet, Manitoba, Canada.

I-D. THEORIES TESTED

In recent years, some of the more important processes associated with contaminant transport in fractured rocks, i.e., hydrodynamic dispersion, matrix diffusion, and adsorption, have been the object of intense experimental and theoretical studies (Skagius and Neretnieks, 1988; Melnyk and Skeet, 1986; Novakowski et al., 1985; Bradbury et al., 1982; Vandergraaf et al., 1982; Grisak and Pickens, 1980; Neretnieks, 1980; Lallemand-Barres and Peaudecerf, 1978). Conceptual models related to the simulation of radionuclide transport in fractured rock, whether based on analytical (Gureghian, 1990; Ahn et al., 1986, Sudicky and Frind, 1982; Rasmuson and Neretnieks, 1981; Tang et al., 1981) or numerical solutions (Huyakorn et al., 1983; Noorishad et al., 1982) and using the discrete fracture approach, are, in the opinion of the authors, adequate for estimating in this instance the key parameters associated with the transport phenomena. A typical model incorporates some or all of the following characteristics:

- One or two-dimensional transport in a single fracture or in multiple planar fractures. The inlet concentration boundary condition, which may be of the first type (Dirichlet) or third type, should also handle two types of release modes in time, i.e., step and band.

The outlet boundary condition may be of the semi-infinite type or second type (i.e., finite).

- One-dimensional diffusion through pores and microfissures in the rock matrix surrounding the fracture. The rock matrix may be of infinite or finite thickness, depending on whether the system considered includes a single-plane fracture or a system of parallel fractures.
- Idealized geometry of the contaminant source which may correspond to a point, patch, or Gaussian.
- Steady-state fluid velocity.
- Longitudinal and transversal dispersion in the fracture.
- Surface adsorption on fracture walls and adsorption in the rock matrix described by a linear equilibrium isotherm.
- Radioactive decay (sink term).

Such a model can be validated using the experiments discussed in this document.

I-E. VALIDATION ASPECTS

A logical series of experiments was designed to calibrate and test the model one parameter at a time. This procedure is outlined below. The first requirement was to set up a parallel and uniform hydraulic gradient as described later in Section I-F.2.1. The experimental/calibration methodology described below is also summarized in Table I-1, where A and B denote the concentrations in the fracture and rock, respectively.

Table I-1. Matrix of Experiments and Simulations for Large Block

Parameter (TBD)*	Tracer	Tracer Sorption R, R′	Fluid Velocity	Type/ Dimension	Tracer Injection Width	Release in Time	Output Function
a_L (L)	Uranine	= 1	High	1-D	Full	1,2**	A = f(t)
D_p (L^2T^{-1})	Uranine	= 1	Low	1-D	Full	1,2**	A = f(t)
K_f (L), K_r (L^3M^{-1})	Cs-137	TBD	N/A	Static Batch	N/A	N/A	K_f (SSA, t)
R, R′	Cs-137	≥ 1	High	1-D	Full	2**	A = f(t) and/or B = f(x,z,t)

*TBD = to be determined.
**1 = Step; 2 = Band.
N/A = not applicable
SSA = Specific Surface Area

I-E.1 Nonadsorbing Tracer Used to Determine Hydrodynamic Dispersion and Matrix Diffusion Coefficients

In order to determine dispersive and diffusive coefficients, experiments were performed with a tracer that would not chemically interact with the rock (e.g., uranine or tritium ^3H). These tracers travel at the same velocity as the fluid without any retardation. AECL provided a value for average rock porosity, ϕ, to use as input in the simulations (Section I- F.2.2).

I-E.1.1 Determination of Longitudinal Dispersivity, (a_L): One-Dimensional Transport

The **longitudinal dispersivity, a_L,** is the first parameter to be determined, because it has a primary role in dictating the shape of the breakthrough curves related to this nonreacting solute, particularly when the matrix diffusion effects play a minor role on the transport process in the fracture, given the short duration (approximately 2-1/2 days) of the experiment. To do this, other competing phenomena that would affect the resulting breakthrough curves and spatial distributions had to be eliminated or at least minimized. Accordingly, high fluid velocity had to exist in the fracture to minimize matrix diffusion. Also, the tracer had to be introduced across the entire width of the fracture to minimize the effect of any transverse dispersion. The tracer source could be either a step or a band release in time.

Next, the tracer breakthrough [concentration (A) versus time (t)] from the experiment was plotted. The computer code was run, and the value of a_L was adjusted until an acceptable fit occurred. This calibrated value of a_L was used in all subsequent code runs.

I-E.1.2 Determination of Matrix Diffusion Coefficient, (D_p): One-Dimensional Transport

The next step was to decrease the fracture flow rate such that **matrix diffusion** became more predominant, allowing calibration of the value of the coefficient, $\mathbf{D_p}$. After reversion to a one-dimensional situation introducing the tracer across the entire fracture width, the breakthrough at the outlet was plotted and, using the a_L from above, the code for D_p was calibrated.

I-E.2 Adsorbing Tracer Used to Study Sorption Coefficients

The final experiment involved a tracer that would chemically react with the rock and thus be retarded and travel slower than the fluid. An example is cesium (Cs-137). Therefore, this experiment took a much longer time than the one described in Section I-E.1. This experiment enabled validation of the computer code(s) as opposed to the calibrations done up to this stage. This is because the values of the adsorption coefficient(s), K_f and K_r, for the fracture and rock respectively, could be measured independently and used as inputs in the model.

I-E.2.1 Static Experiments

AECL performed independent, static, batch-type experiments to determine the sorptive properties of Cs-137 on the rock. These experiments were done simultaneously with the block migration ones. Upon completion, AECL provided Battelle with a fracture surface adsorption coefficient, K_f [cm], and an appropriate rock matrix adsorption coefficient, K_r [mL/g].

I-E.2.2 Validating the Code(s)

The high-velocity experiment described in Section I-E.1.1 was repeated using Cs-137 as the tracer. The high velocity minimized matrix diffusion as well as speed up what would otherwise be an extremely slow transport problem. The breakthrough curve [A = f(t)] was measured until the peak concentration arrived at the fracture outlet. At this point, the experiment was discontinued. The fracture was taken apart, and the spatial distribution [A = f(x)] of the Cs-137 was determined by autoradiography.

In both the temporal and spatial cases, the K_f and K_r values from Section I-E.2.1 were used to simulate the transport and compare the calculated spatial distribution (or temporal breakthrough) to the experimental results obtained in the previous paragraph. The closeness of this comparison reflected the appropriateness of the simplifying assumptions made in the mathematical model(s) to approximate the relevant transport phenomena.

I-F. BACKGROUND INFORMATION

I-F.1 Geological Information

The mineralogical composition of this particular block is not yet available. However, the medium- to coarse-grained pink granite from the quarry area has been analyzed and reported and is given in Table I-2 (Tammemagi et al., 1980). Analysis of the fracture in filling material in granite reveals that the major constituents are generally calcite and silica with smaller amounts of K-feldspar minerals. Clay minerals are occasionally identified at the fracture surface and amorphous iron oxides are generally present (Tammemagi et al., 1980).

Table I-2. Mineralogical Composition of Lac du Bonnet Granite in Percent

Quartz	28.5
Corundum	1.6
Zircon	0.03
Orthoclase	28.3
Albite	32.32
Anorthite	4.61
Magnetite	0.84
Apatite	0.09
Calcite	0.2
Biotite	2.94
Sphene	0.5

I-F.2 Hydrogeological Information

I-F.2.1 Simplifying Modifications Required for Model Calibration/Validation

The following simplifications were made:

(a) Symmetry

Symmetry of the hydraulic gradient and tracer transport was maintained about the center-line of the fracture.

(b) Hydraulic/Gradient

AECL devised a way to establish a hydraulic gradient across the entire fracture width (as opposed to a dipolar one). A reservoir is created across each of the two open edges of the fracture and a uniform gradient is applied between them.

I-F.2.2 Rock Porosity and Density

Measurements made on a similar granite block gave a porosity ϕ of 2.72×10^{-3} for the first cm of rock immediately adjoining the fracture surface, whereas an average porosity of 1.96×10^{-3} was obtained for the next 9 cm (Melnyk and Skeet, 1986). For the mathematical simulations performed in this report, a weighted average of the above porosities was used, i.e., $\phi = 2 \times 10^{-3}$. The density of the rock ρ_r is 2.65 g/mL.

I-F.2.3 Rock Diffusivity

It was important to establish the value of the rock pore diffusivity D_p, which along with porosity is an important parameter that governs the tracer diffusion rate into the rock matrix (see Equations A-3 and A-4 in Appendix A). Pore diffusivity, defined as the product of molecular diffusion of a typical nuclide in water D_d and the geometric factor (δ_d/τ^2) (see Neretnieks, 1980), varies primarily with pressure and temperature of the rock. Literature values reported by Neretnieks (1980) indicate that the value of the geometric factor for granite varies between 0.15 and 0.6 at atmospheric pressure and between 0.06 and 0.2 at 100 bars. At this stage, the best estimate of the rock diffusivity was found in the literature. The definitions used in this report are the same as those used in recent measurements of cesium and strontium diffusion in biotite gneiss (Skagius and Neretnieks, 1988). The literature values shown in Table I-3 are consistent with those quoted in the above paper.

I-F.3 Geochemical Information

I-F.3.1 Rock and Ground-Water Composition

The chemical composition of the pink granite from the area of the commercial quarry from which the block was taken is given in Table I-4. For comparison, the range of chemical compositions of the granite in this batholith is also included (Tammemagi et al., 1980). The ground-water composition is given in Table I-5. This is a standard synthetic granitic ground water (GGW) used by AECL in most of these types of experiments. This composition minimizes the chemical potential gradients between fluid and rock which, in turn minimizes chemical reactions that lead to dissolution and precipitation.

Table I-3. Literature Values of Relevant Diffusion Parameters

Tracer	D_e (m^2/s)	D_p (cm^2/h)
Cesium	$1x10^{-13}$	$1.8x10^{-3}$
Iodide	$1x10^{-14}$	$1.8x10^{-4}$
Other non-adsorbing	$1x10^{-14}$	$1.8x10^{-4}$

I-F.3.2 Bulk Rock Distribution Coefficient

The bulk adsorption coefficient, K_r, of cesium in the rock was estimated in previous experiments performed by AECL to be 0.34 mL/g. Based on Equation A-6b (Appendix A), the corresponding rock retardation factor, R', was determined to be 451.

I-F.4 Geophysical Information

No geophysical information is presently available.

Table I-4. Chemical Composition of Lac du Bonnet Granite

Element/Oxide	Pink Granite	Lac du Bonnet Granite
	(Concentrations in Percent)	
SiO_2	72.40	76.9 - 68.1
Al_2O_3	14.40	16.5 - 12.6
Fe_2O_3	0.79	1.40 - 0.45
FeO	0.88	1.60 - 0.22
TiO_2	0.24	0.27 - 0.04
MgO	0.47	0.71 - 0.11
CaO	1.19	1.81 - 0.57
Na_2O	3.55	4.55 - 2.98
K_2O	5.03	5.84 - 3.78
MnO	0.04	0.09 - 0.012
	(Concentrations in µg/g)	
Ba	879	1718 - 391
Sr	215	782 - 28
Zr	203	300 - 118
P	175	742 - 2
C	218	710 - 115
Sn	8	13 - 2
Cs	1.9	13 - 0.2
Rb	206	327 - 85
Tl	1.4	2 - <1
Y	4	14 - 1
Li	35	110 - 17
Th	36	36 - 5
U	7	26 - 1
Be	1.5	3 - 0.8
Ga	29	34 - 23
Hf	2	7 - 1.5
Pb	23	27 - 11
Total	99.25%	

Table I-5. Chemical Composition of Synthetic Granitic Ground Water (GGW)

Ion	Concentration (mg/L)
Na^+	8.3
K^+	3.5
Mg^{2+}	3.9
Ca^{2+}	13.0
Cl^-	5.0
SO_4^{2-}	8.6
NO_3^-	0.62
F^-	0.1
pH	7.3

II. EXPERIMENTAL DESIGN

II-A. PARAMETERS MEASURED

First, the block dimensions were determined. The volumetric flow rate was established at 20 mL/h and the known tracer concentration at the inlet was used to normalize the outlet concentrations. During the experiment, the outlet concentrations were measured as a function of time. Other input parameters such as porosity and surface and bulk adsorption coefficients were determined separately in independent experiments. Finally, at the conclusion of the migration experiments, concentrations could be measured as a function of space on the fracture walls as well as in the rock matrix.

II-B. SPATIAL AND TEMPORAL SCALES

The large block, LB-2, is 91.5 cm long (in the flow direction), 86.5 cm wide, and 49.0 cm high. The fracture aperture was estimated from the volume of water required to completely fill the fracture to average approximately 800 μm (0.08 cm).

The uranine (nonadsorbing) experiment described in Sections IV-A.1 and IX-A lasted 60 hours (2.5 days). In contrast, the cesium (adsorbing) experiment described in Sections IV-A.3 and IX-B lasted approximately 360 hours (15 days).

II-C. EXPERIMENTAL SETUP

The granite block contained a single, natural fracture. This block was positioned to make the fracture approximately horizontal (Figure II-1). Suitable reservoirs were designed so that as uniform a gradient as possible could be imposed across the entire width of the fracture. The outside surfaces of the block, as well as the edges of the fracture on the 91.5-cm sides, were coated with a silicone-based rubber (GTE, RTV-108) to avoid evaporation of the transport solution through the porous rock matrix.

Inlet and outlet reservoirs were designed for this quarried block. These reservoirs were attached to the short sides of the block (86.5 cm) and covered the fracture where it intersected these surfaces of the block. This way a uniform gradient could be created across the entire width of the fracture with a path length of 91.5 cm.

The inlet reservoir consisted of a 86.5-cm-long acrylic tube cut lengthwise and fitted with two semicircular acrylic end pieces (Figure II-2). This reservoir covered the inlet of the fracture and contained four ports. In addition, a rubber septum was located at the center of the reservoir so that a syringe could be inserted in the fracture to carry out possible point-source injections. An HPLC-type pump (ISCO model 314, ISCO, Inc., Lincoln, Nebraska, USA) was used to inject the transport solution in the fracture, thus ensuring a very stable flow rate throughout the experiment. For this experiment, a flow rate of 20 mL/h was selected and a continuous injection of a conservative tracer through both ports located at the ends of the inlet reservoir was carried out.

In retrospect, although the inlet reservoir spanned the width of the block, the varying aperture of the fracture did not allow for a uniform flow from the inlet reservoir. In fact, there is some evidence from the postexperimental two-dimensional γ-scanning of the fracture surfaces that the ground water entered the fracture mainly in one location.

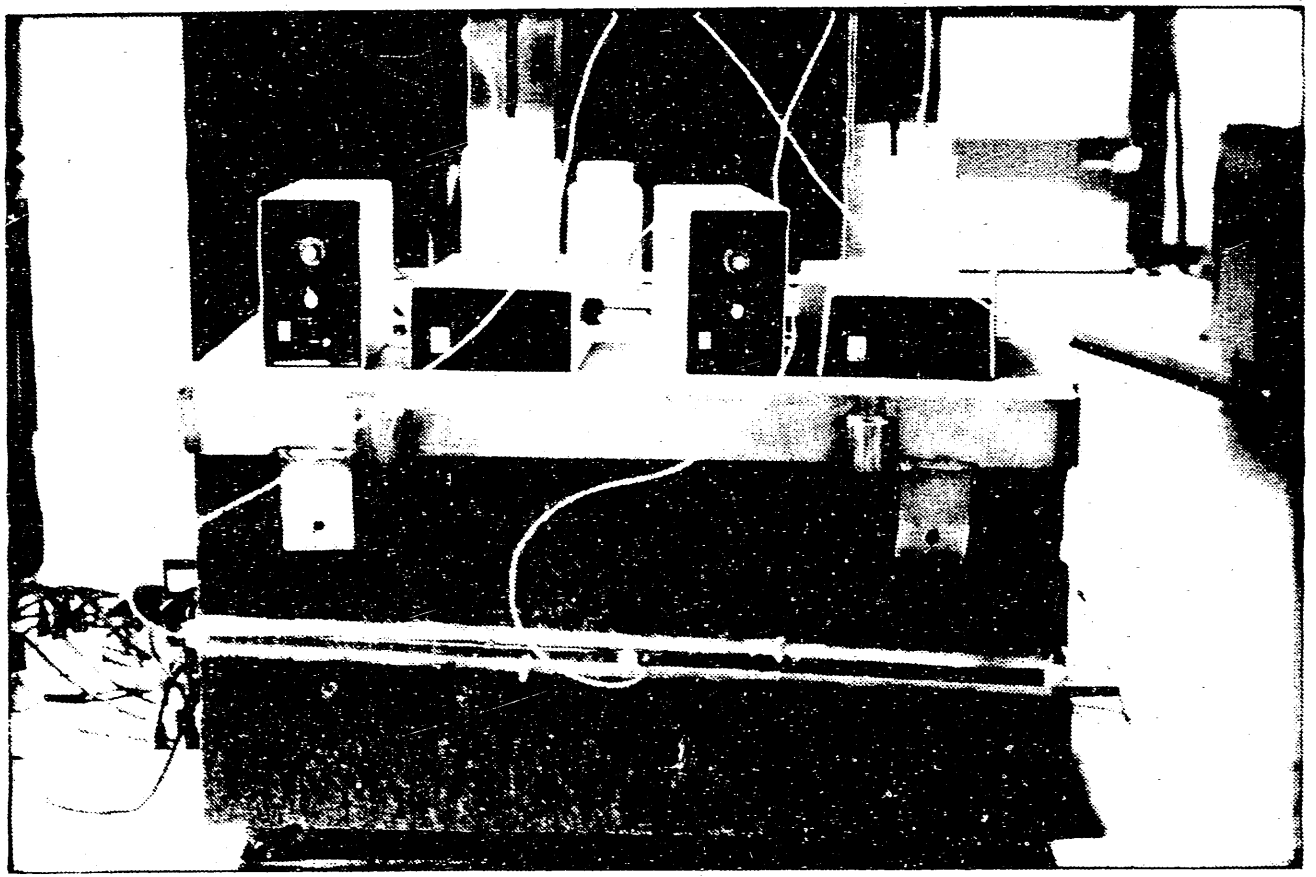

Figure II-1. Granite Block LB-2 Showing Location of Inlet Reservoir. Note Angle of the Fracture

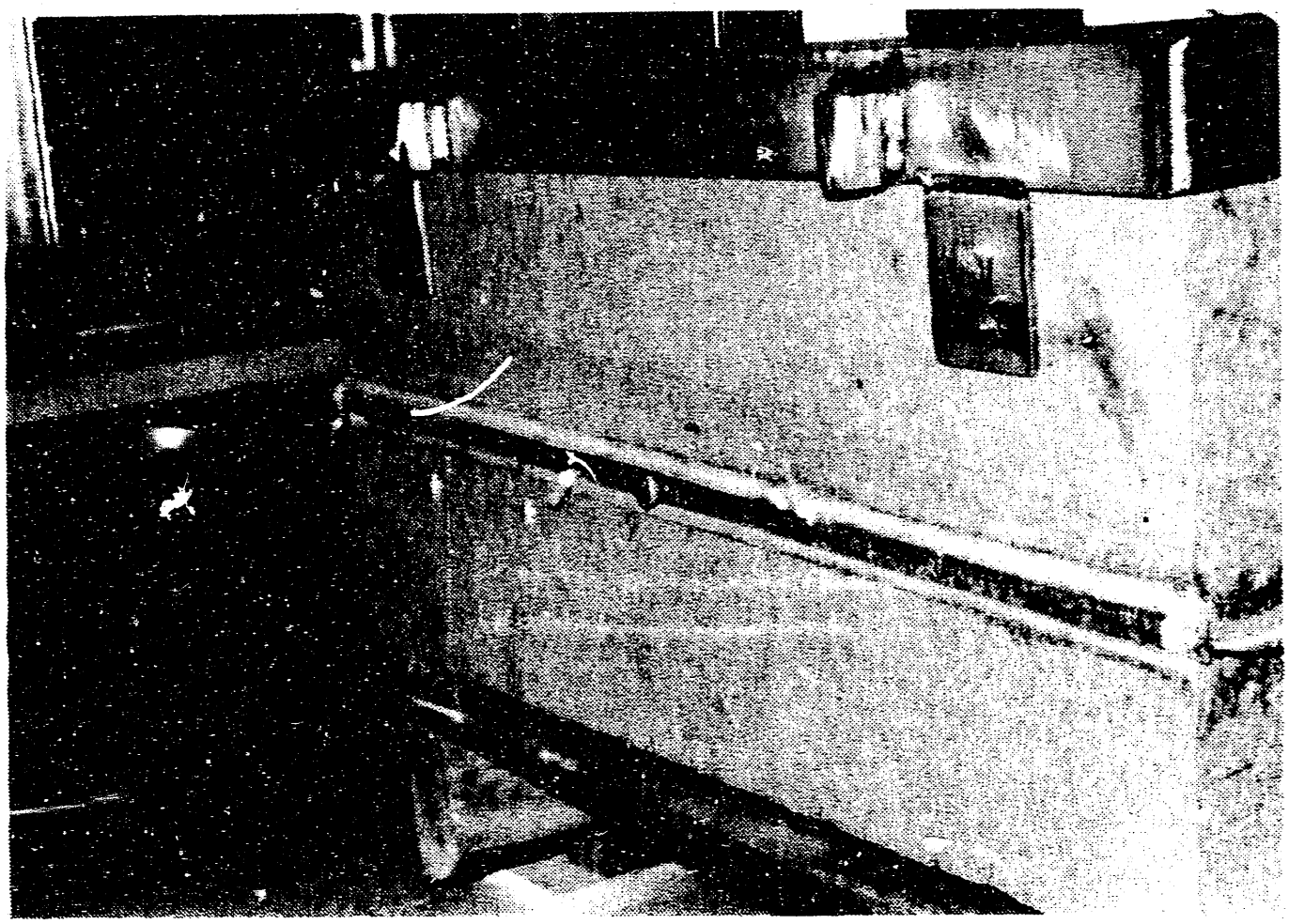

Figure II-2. LB-2 Inlet Reservoir Showing Various Ports and Septum

II-D. SAMPLING STRATEGY

The outlet reservoir consisted of a shallow channel cut into a Plexiglas™ plate. This channel followed the trace of the fracture as it intersected with the exit face of the block. The channel was divided into five compartments of equal length, and each compartment was equipped with a pair of valved inlet and outlet ports. The outlet port of each compartment was hooked up to a separate fraction collector. Figure II-3 shows a schematic of this arrangement. In order to obtain representative values of the breakthrough curves, channeling effects in the fracture were minimized after allowing the transport solution to flow equally to the five compartments. This was accomplished by placing solenoid valves in the lines connecting each outlet port and its companion fraction collector. The flow rate of the ground water through the five different channels was not identical, and this may have resulted in a very slight increase in the fracture aperture as a result of changes in the resistivity of a particular channel. Calculations showed that this increase in aperture was less than 1 μm, and can probably be ignored.

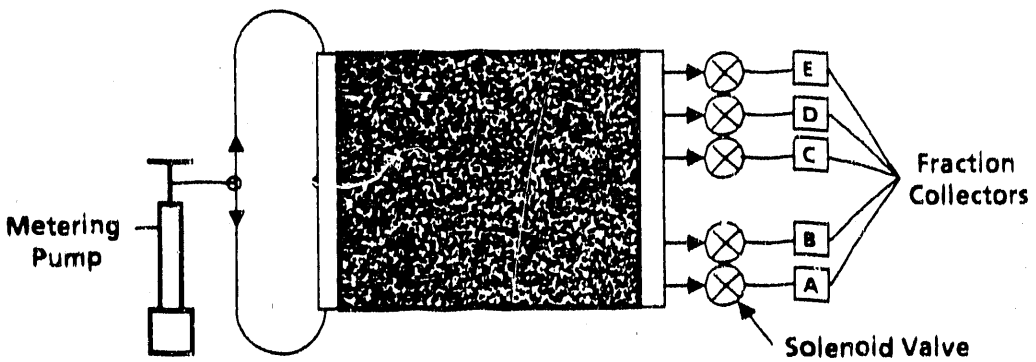

Figure II-3. Schematic Plan View of the Arrangement of the Inlet and Outlet Reservoirs on LB-2

Figure II-4 shows the exit of the fracture before the outlet reservoir was put in place and Figure II-5 shows the actual outlet reservoir and the arrangements of the solenoid valves. The solenoid valves were triggered in sequence after a given number of drops had been collected in each fraction collector. With an average flow velocity of 20 mL/h and a volume of 1 mL (20 drops) collected in each vial, an average of 15 minutes were required to complete a cycle through all five fraction collectors. This time was small enough relative to the total duration of the experiment to justify the use of an average, uniform flow rate.

II-E. INDEPENDENCE BETWEEN DATA SETS

The data sets reported in this report, i.e., uranine and Cs-137, were the results of two distinct experiments using the same granite block.

II-F. BIASES INHERENT IN THE DESIGN

The two halves of the block were not bolted together, but the top half rested on the bottom half. This may have led to some variation in the fracture aperture over the duration of the experiment (see also Section II-D).

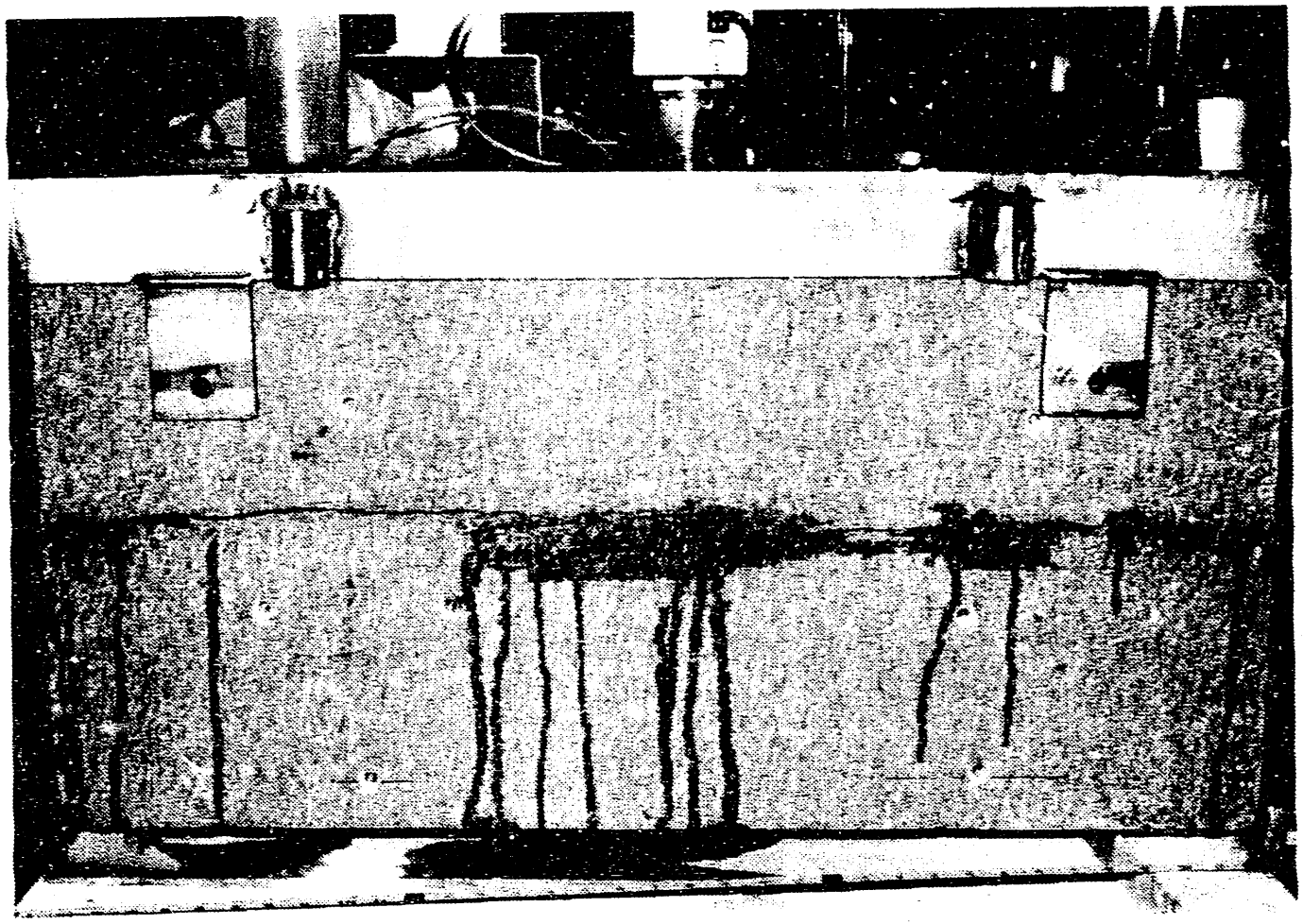

Figure II-4. Exit Face of LB-2 Before Attaching Outlet Reservoir Showing Locations of Maximum Flow in a Nonrestricted Flow Regime

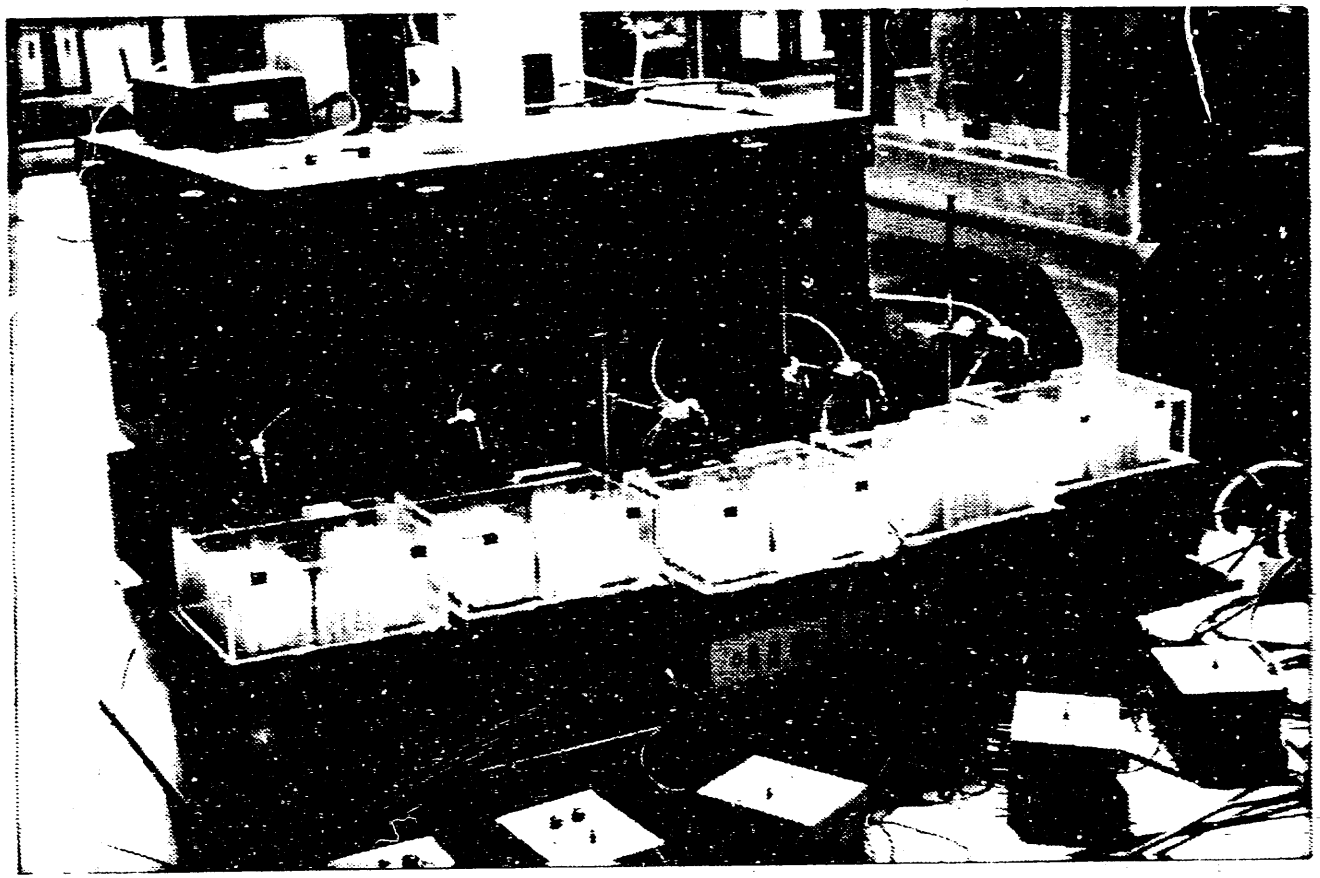

Figure II-5. Outlet Face of Block Showing Fracture Exit and Eluate Collection Arrangement

II-G. COMPLEMENTARY EXPERIMENTS

Other experiments were carried out as a part of this exercise. They are described along with their corresponding mathematical simulations in Section V and in Noronha et al., 1988.

III. CURRENT STATUS AND EXPERIMENTAL SCHEDULE

The experiments are now complete. Breakthrough curves of experimental results are available from the pilot group. Spatial concentrations are not yet available.

IV. EXPERIMENTAL RESULTS

IV-A. RAW DATA

IV-A.1 Uranine Migration

A 2×10^{-5} mole/L solution of Na-fluorescein (uranine) was prepared in dilute granite ground water (GGW), and this nonreactive tracer was injected at a flow rate of 20 mL/h. The uranine concentrations in the eluate were divided by that in the starting solution to obtain normalized concentrations. Th normalized concentrations in the fracture were plotted versus time to obtain breakthrough curves (A/A^0 versus t, where A^0 refers to the concentration of the tracer at the source at time equals zero) and are shown in Figure IV-1. The corresponding tabulated values are given in Table IV-1. The five elution profiles that were obtained are not identical. This indicates that the fracture aperture varies across the width of the fracture. This is not an unexpected observation because the fracture in this experiment is a natural fracture, and these fractures seldom if ever have a constant aperture.

IV-A.2 Static Cesium Sorption Experiments

Static sorption experiments for Cs-137 were carried out on representative natural granite fracture surfaces taken from the same area as the granite block used in the migration experiment. Sorption was studied as a function of cesium concentration (10, 100, 1,000 mg Cs/L), surface area-to-volume ratio (0.54, 0.81, 1.62 cm^{-1}), and time (0.1, 0.3, 1, 3, 10, 30, and 100 d). The experimental method has been described by Abry et al., 1982. The results for the 1,000-mg Cs/L cesium concentration are shown in Table IV-2.

Based on the short time span of the experiment and the rather important retardation effects that Cs-137 is likely to undergo in the rock matrix of interest, both mechanisms associated with the transport of this species (i.e., radioactive decay and rock matrix diffusion) may for the purpose of our discussions be safely neglected. In the absence of retardation effects in the fracture and in view of the data reported in Section IV-B, the residence time ($t_T = L/u$, see Ogata and Banks, 1961) of Cs-137 would correspond to approximately 1 day. Because the stationary (or saddle) point on the representative average breakthrough curve corresponding to $A/A^0 = 0.5$ (see Table IV-3) indicates a value for t_T corresponding to approximately 3 days, we may deduce that the retardation factor in the fracture would be equivalent to the ratio of these two residence travel times (i.e., R = 3). This estimate is supported by the fact that the value of $K_f = 0.06$ cm reported in Table IV-2 corresponds to an average value for surface-area-to-volume ratio of 0.81 cm^{-1}, which would yield an almost identical retardation factor based on Equation A-6a (see Appendix A) and a fracture thickness of 6.23×10^{-2} cm. Although the choice of this parameter value $K_f = 0.06$ cm bears some uncertainty, it was adopted in the mathematical prediction described in Section IX-B.

IV-A.3 Cesium Migration

The conditions for this experiment were described in Section II-C. A flow rate of 20 mL/h was used, and the eluent was collected in 1-mL increments. A tracer solution containing 1.2×10^6 Bq/L of Cs-137 was used as the sorbing tracer. Due to time constraints, advantage was taken of the nonlinear sorption behavior of cesium (Vandergraaf et al., 1986), so that 1,000 mg/L of inactive cesium was added to depress cesium sorption and to decrease the retardation of this element in the fracture. The outlet concentrations were determined by gamma spectrometry using a Ge(Li) detector. Cs-137 breakthrough curves for each of the five outlet ports are shown in Figure IV-2. The corresponding tabulated values are given in Table IV-3.

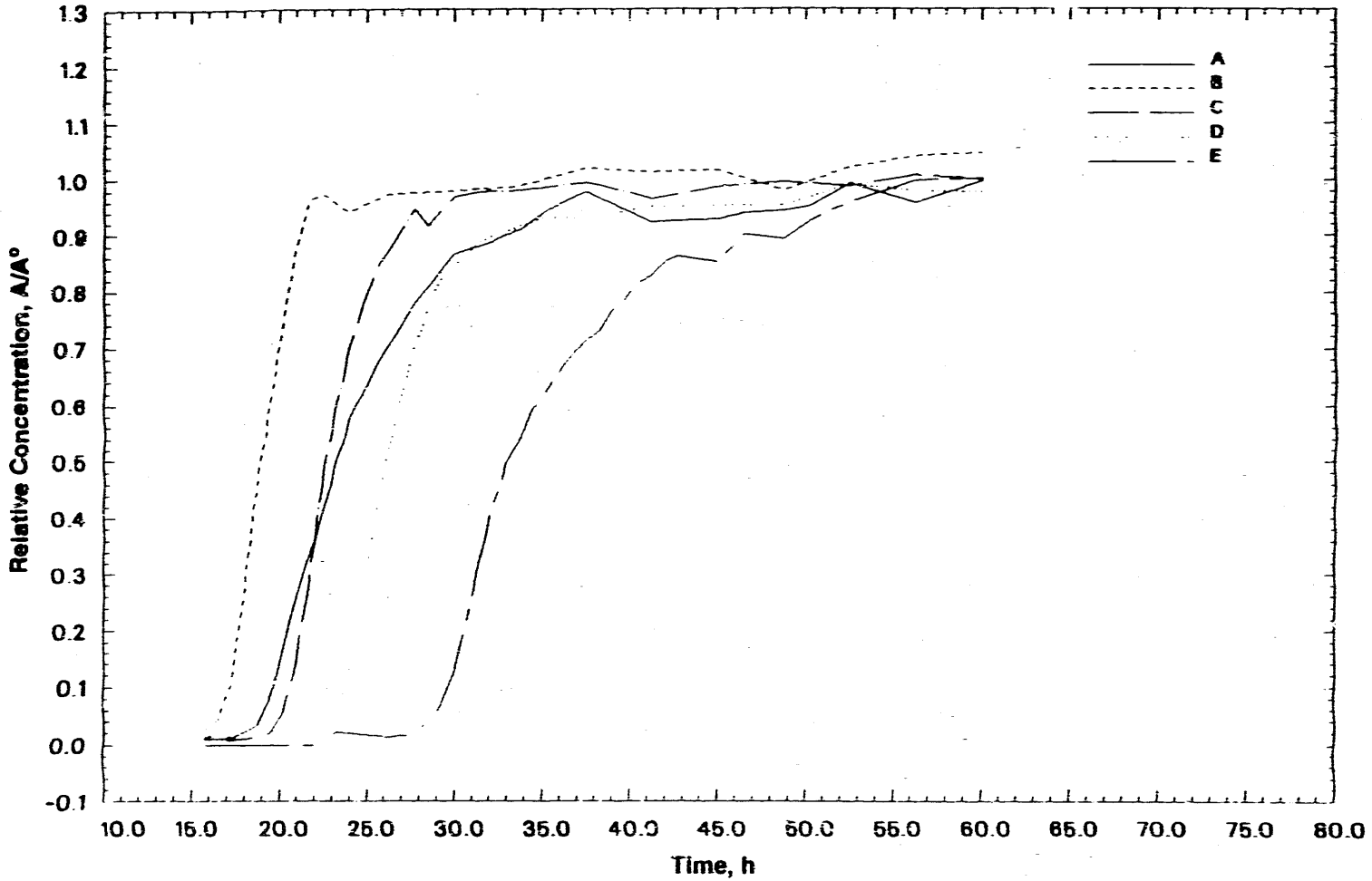

Figure IV-1. Experimental Uranine Elution Profiles for the Longitudinal Dispersivity Experiment. A Through E Refer to the Sampling Locations Shown in Figure II-3

Table IV-1. Experimental Uranine Relative Concentration Breakthrough Curves for the Longitudinal Dispersivity Experiment. A through E Refer to the Five Sampling Locations Shown in Figure II-3.

Time (hours)	A/A°					Average A/A°
	A	B	C	D	E	
15.750	0.0119	0.0254	0.0093	0.0102	0.0000	0.0114
16.500	0.0111	0.0412	0.0112	0.0093	0.0000	0.0146
17.250	0.0104	0.1014	0.0075	0.0085	0.0000	0.0255
18.000	0.0216	0.2615	0.0115	0.0093	0.0000	0.0608
18.750	0.0328	0.4633	0.0129	0.0101	0.0000	0.1038
19.500	0.0778	0.6011	0.0204	0.0087	0.0000	0.1416
20.250	0.1661	0.7516	0.0550	0.0074	0.0000	0.1960
21.000	0.2597	0.8780	0.1437	0.0105	0.0000	0.2584
21.750	0.3359	0.9626	0.2928	0.0135	0.0000	0.3210
22.500	0.4078	0.9740	0.4724	0.0166	0.0000	0.3741
23.250	0.4952	0.9573	0.5929	0.0393	0.0210	0.4212
24.000	0.5758	0.9406	0.6983	0.1245	0.0194	0.4717
24.750	0.6187	0.9518	0.7702	0.2549	0.0177	0.5227
25.500	0.6652	0.9629	0.8374	0.4008	0.0160	0.5765
26.250	0.7046	0.9740	0.8715	0.5254	0.0142	0.6179
27.000	0.7415	0.9751	0.9089	0.6189	0.0158	0.6520
27.750	0.7784	0.9763	0.9463	0.7022	0.0173	0.6841
28.500	0.8075	0.9774	0.9163	0.7693	0.0403	0.7022
29.250	0.8367	0.9785	0.9427	0.8252	0.0634	0.7293
30.000	0.8659	0.9797	0.9691	0.8439	0.1265	0.7570
30.750	0.8732	0.9813	0.9736	0.8667	0.2171	0.7824
31.500	0.8805	0.9829	0.9780	0.8894	0.3249	0.8112
32.250	0.8902	0.9846	0.9789	0.8978	0.4246	0.8352
33.000	0.9000	0.9862	0.9797	0.9062	0.4960	0.8536
33.750	0.9098	0.9878	0.9805	0.9146	0.5442	0.8674
34.500	0.9264	0.9943	0.9833	0.9236	0.5920	0.8839
35.250	0.9431	1.0008	0.9862	0.9325	0.6244	0.8974
36.000	0.9547	1.0073	0.9889	0.9314	0.6593	0.9083
36.750	0.9664	1.0138	0.9916	0.9304	0.6868	0.9178
37.500	0.9780	1.0203	0.9943	0.9293	0.7126	0.9269

Table IV-1. (Continued)

Time (hours)	A/A°					Average A/A°
	A	B	C	D	E	
38.250	0.9672	1.0189	0.9892	0.9335	0.7308	0.9279
39.000	0.9563	1.0174	0.9840	0.9377	0.7638	0.9318
39.750	0.9454	1.0159	0.9789	0.9420	0.7859	0.9336
40.500	0.9345	1.0145	0.9720	0.9462	0.8154	0.9365
41.250	0.9236	1.0130	0.9650	0.9504	0.8285	0.9361
42.000	0.9246	1.0138	0.9696	0.9509	0.8515	0.9421
42.750	0.9255	1.0146	0.9741	0.9514	0.8629	0.9457
45.000	0.9285	1.0171	0.9878	0.9528	0.8526	0.9478
46.500	0.9390	1.0024	0.9911	0.9535	0.9014	0.9575
48.750	0.9439	0.9805	0.9959	0.9545	0.8936	0.9537
50.250	0.9520	0.9971	0.9930	0.9691	0.9268	0.9676
52.500	0.9927	1.0220	0.9886	0.9911	0.9589	0.9906
56.250	0.9577	1.0407	1.0C ,1	0.9805	0.9990	0.9972
60.000	0.9976	1.0463	1.0000	0.9772	1.0010	1.0044

Table IV-2. Calculated K_f Values (cm) for 1,000 mg Cs/L Concentration

Time (days)	Surface Area/Volume (cm^{-1})		
	0.54	0.81	1.62
0.1	----	0.13	----
0.3	0.11	----	0.19
1.0	----	0.03	----
3.0	0.14	**0.06**	0.14
10.0	0.12	0.09	0.29
30.0	0.21	0.18	0.34
100.0	0.44	0.38	0.53

Migration of Cs-137 through the fracture was retarded. Its velocities in the different channels were compared with those of uranine and an average retardation factor, R, of 3.27 was determined. This corresponds to a K_f value of 0.071 cm, which is reasonably close to the value of 0.06 cm selected from Table IV-1.

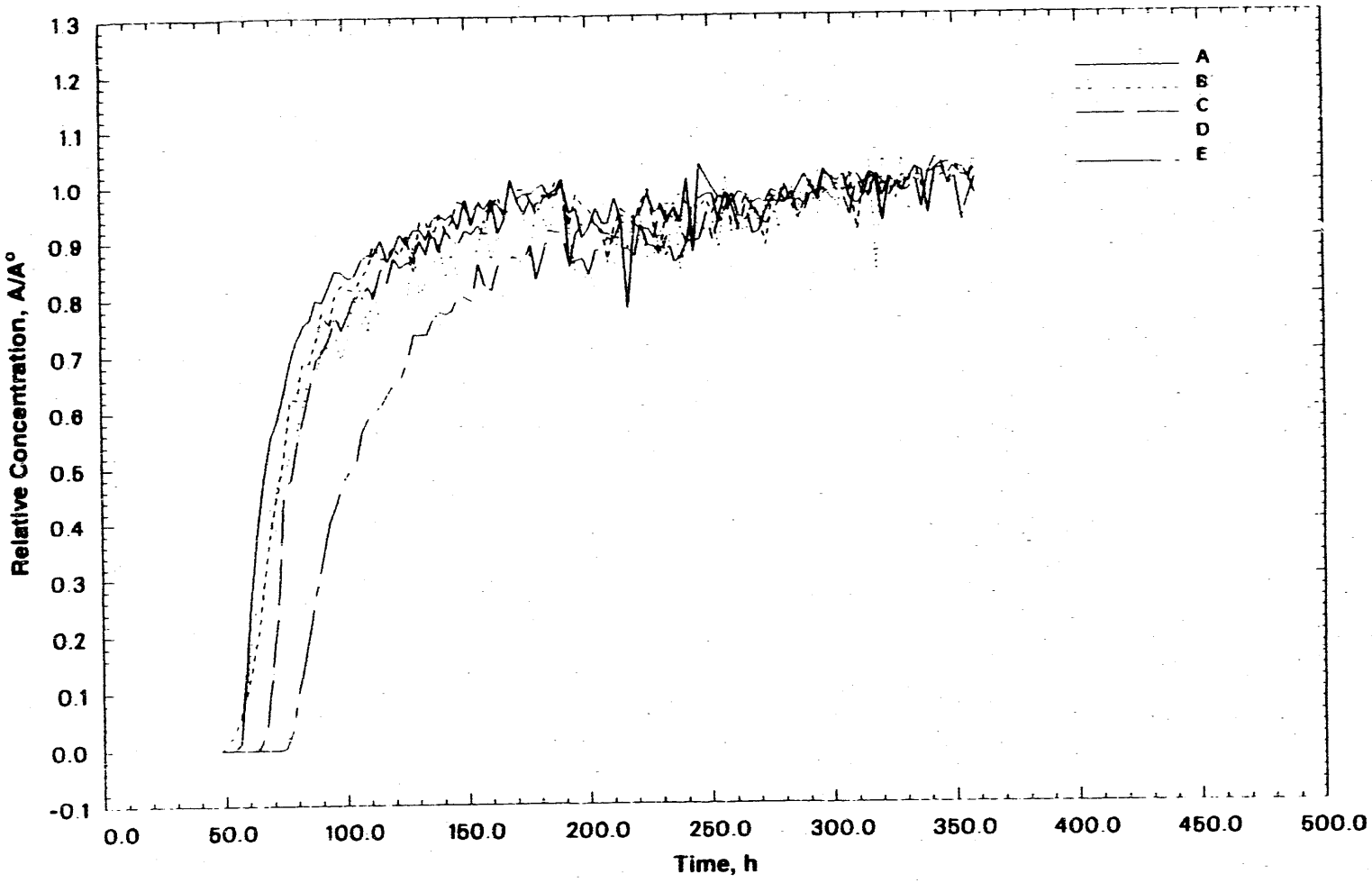

Figure IV-2. Experimental Elution Profiles for Cs-137 Migration

Table IV-3. Experimental Cs-137 Relative Concentration Breakthrough Curves for the Sorption Migration Experiment. A Through E Refer to the Five Sampling Locations Shown in Figure II-3.

Time (hours)	A/A°					Average A/A°
	A	B	C	D	E	
48.150	0.0000	0.0000	0.0000	0.0000	0.0000	0.0000
50.825	0.0000	0.0102	0.0000	0.0000	0.0000	0.0020
53.500	0.0000	0.0296	0.0000	0.0000	0.0000	0.0059
56.175	0.0106	0.0574	0.0000	0.0130	0.0000	0.0162
58.850	0.1460	0.0953	0.0000	0.1200	0.0000	0.0723
61.525	0.2912	0.1554	0.0000	0.2149	0.0000	0.1323
64.200	0.4027	0.2137	0.0045	0.2893	0.0000	0.1820
66.875	0.4894	0.3108	0.0330	0.3823	0.0000	0.2431
69.550	0.5540	0.3987	0.1347	0.3870	0.0000	0.2949
72.225	0.5885	0.4579	0.2507	0.4753	0.0000	0.3545
74.900	0.6354	0.5273	0.4674	0.4949	0.0019	0.4254
77.575	0.6786	0.6244	0.4764	0.5256	0.0331	0.4694
80.250	0.7248	0.6207	0.5388	0.5647	0.0993	0.5097
82.925	0.7540	0.6892	0.5932	0.6140	0.1599	0.5620
85.600	0.7611	0.6864	0.6441	0.6744	0.2233	0.5978
88.275	0.7965	0.7253	0.6922	0.6688	0.2876	0.6341
90.950	0.7920	0.7752	0.7047	0.7098	0.3425	0.6648
93.625	0.8195	0.7493	0.7306	0.7153	0.4021	0.6834
96.300	0.8478	0.8030	0.7681	0.7349	0.4314	0.7170
98.975	0.8460	0.8233	0.7449	0.6884	0.4721	0.7149
101.650	0.8336	0.8150	0.7725	0.7507	0.4938	0.7331
104.325	0.8398	0.8141	0.8011	0.7907	0.5024	0.7496
107.000	0.8655	0.8372	0.7993	0.8177	0.5639	0.7767
109.675	0.8761	0.8501	0.8198	0.7414	0.5847	0.7744
112.350	0.8743	0.8945	0.8011	0.8130	0.5970	0.7960
115.025	0.9027	0.8686	0.8510	0.7600	0.6112	0.7987
117.700	0.8628	0.8696	0.8269	0.7572	0.6306	0.7894
120.375	0.8823	0.8899	0.8689	0.7851	0.6500	0.8152
123.050	0.9115	0.8733	0.8519	0.8214	0.6566	0.8229
125.725	0.8938	0.9093	0.8599	0.7860	0.6840	0.8266
128.400	0.9204	0.8464	0.8635	0.8940	0.7360	0.8521
131.075	0.9204	0.9343	0.9010	0.8028	0.7342	0.8585
133.750	0.9027	0.9343	0.8760	0.8279	0.7342	0.8550
136.425	0.9381	0.9056	0.9188	0.8447	0.7597	0.8734

Table IV-3. (Continued)

Time (hours)	A/A°					Average A/A°
	A	B	C	D	E	
139.100	0.9469	0.9436	0.8805	0.8930	0.7720	0.8872
141.775	0.9381	0.9195	0.9188	0.8344	0.7682	0.8758
144.450	0.9469	0.9343	0.9010	0.8772	0.7739	0.8867
147.125	0.9204	0.9713	0.8921	0.8344	0.8070	0.8850
149.800	0.9735	0.9621	0.9188	0.8530	0.7975	0.9010
152.475	0.9292	0.9251	0.9099	0.8651	0.7928	0.8844
155.150	0.9646	0.9713	0.9277	0.8847	0.8571	0.9211
157.825	0.9558	0.9528	0.9099	0.9395	0.8202	0.9157
160.500	0.9735	0.9528	0.9723	0.8651	0.8117	0.9151
163.175	0.9115	0.9806	0.9634	0.9079	0.8543	0.9235
165.850	0.9381	0.9436	0.9456	0.8823	0.8647	0.9148
168.525	1.0088	0.9991	0.9545	0.8567	0.8713	0.9381
171.200	0.9735	0.9898	0.9723	0.9284	0.8675	0.9463
173.875	0.9823	0.9898	0.9456	0.9488	0.8553	0.9444
176.550	0.9823	0.9713	0.9723	0.8670	0.8912	0.9368
179.225	0.9912	0.9621	0.9456	0.9674	0.8297	0.9392
181.900	1.0000	0.9806	0.9723	0.9395	0.8732	0.9531
184.575	0.9735	0.9713	0.9813	0.9107	0.9167	0.9507
187.250	0.9823	1.0083	0.9902	0.9860	0.9130	0.9760
189.925	1.0000	0.9991	1.0080	0.9558	0.9120	0.9750
192.600	0.9469	0.9251	0.8510	0.9256	0.8553	0.9008
195.275	0.9558	0.9806	0.9099	0.8372	0.8638	0.9094
197.950	0.9027	0.9621	0.9277	0.8419	0.8657	0.9000
200.625	0.9204	0.9528	0.9367	0.8223	0.8363	0.8937
203.300	0.9558	0.9251	0.9277	0.8521	0.8808	0.9083
205.975	0.9292	0.9158	0.9099	0.8800	0.8808	0.9031
208.650	0.9292	0.8631	0.9099	0.8595	0.9035	0.8930
211.325	0.9735	0.9241	0.9010	0.8512	0.8921	0.9084
214.000	0.9292	0.9528	0.9367	0.9581	0.8846	0.9323
216.675	0.7761	0.9436	0.9367	0.8819	0.8836	0.8844

Table IV-3. (Continued)

Time (hours)	A/A°					Average A/A°
	A	B	C	D	E	
219.350	0.9381	0.9343	0.9277	0.9488	0.8685	0.9235
222.025	0.9469	0.9621	0.9188	0.9395	0.9253	0.9385
224.700	0.9823	0.9898	0.9188	0.8642	0.8893	0.9289
227.375	0.9469	0.9214	0.9010	0.8670	0.8865	0.9045
230.050	0.9558	0.8714	0.9634	0.9144	0.8675	0.9145
232.725	0.9292	0.9621	0.9367	0.8623	0.9063	0.9193
235.400	0.9558	0.9713	0.9545	0.9674	0.8590	0.9416
238.075	0.9292	0.9806	0.9188	0.8456	0.8666	0.9082
240.750	1.0088	0.9621	0.8912	0.8977	0.8950	0.9309
243.425	0.8752	0.9621	0.9723	0.9237	0.8950	0.9257
246.100	1.0354	0.9528	0.9723	0.9051	0.8997	0.9531
248.775	1.0088	0.9713	0.9813	0.9228	0.9461	0.9661
251.450	0.9912	0.9436	0.9813	0.9302	0.8940	0.9481
254.125	0.9735	0.9806	0.9277	0.8828	0.9376	0.9404
256.800	0.9735	0.9621	0.9545	1.0140	0.9839	0.9776
259.475	0.9646	0.9251	0.9813	0.8940	0.9555	0.9441
262.150	0.9841	0.9408	0.9376	0.9256	0.9149	0.9406
264.825	0.9788	0.9325	0.9732	0.9079	0.9622	0.9509
267.500	0.9619	0.9593	0.9554	0.9516	0.9082	0.9473
270.175	0.9708	0.9389	0.9376	0.9302	0.9130	0.9381
272.850	0.9637	0.8871	0.9260	0.9507	0.9470	0.9349
275.525	0.9867	0.9685	0.9358	0.9805	0.9688	0.9681
278.200	0.9788	0.9815	0.9661	0.9163	0.9622	0.9610
280.875	0.9664	0.9907	0.9634	1.0056	1.0000	0.9852
283.550	0.9690	0.9621	0.9839	0.9972	0.9555	0.9736
286.225	0.9929	0.9352	0.9411	0.9423	0.9688	0.9561
288.900	1.0159	0.9639	0.9465	1.0149	0.9603	0.9803
291.575	0.9947	1.0019	0.9795	0.9898	0.9773	0.9886
294.250	0.9664	0.9667	0.9786	0.9395	0.9839	0.9670
296.925	1.0168	0.9796	0.9893	0.9926	1.0237	1.0004

Table IV-3. (Continued)

Time (hours)	A/A°					Average A/A°
	A	B	C	D	E	
299.600	1.0080	0.9907	0.9715	1.0326	1.0066	1.0019
302.275	1.0009	0.9963	0.9670	0.9451	0.9839	0.9786
304.950	1.0150	0.9833	0.9732	1.0047	0.9991	0.9951
307.625	0.9699	1.0194	0.9393	0.9935	0.9849	0.9814
310.300	0.9602	0.9121	1.0054	1.0502	1.0151	0.9886
312.975	0.9735	1.0000	0.9813	1.0298	0.9934	0.9956
315.650	1.0124	0.9685	0.9813	1.0447	1.0180	1.0050
318.325	1.0044	1.0167	1.0116	0.8391	1.0104	0.9764
321.000	0.9292	0.9954	1.0000	1.0437	0.9735	0.9884
323.675	1.0053	0.9981	0.9741	1.0000	1.0076	0.9970
326.350	0.9973	0.9676	0.9964	0.9842	0.9905	0.9872
329.025	0.9858	1.0129	0.9973	1.0447	0.9839	1.0049
331.700	1.0053	1.0000	1.0062	0.9405	0.9877	0.9879
334.375	1.0257	1.0278	1.0277	1.0177	1.0066	1.0211
337.050	1.0212	0.9944	1.0107	0.9888	0.9517	0.9934
339.725	0.9407	0.9898	1.0161	0.9795	1.0161	0.9884
342.400	1.0239	0.9972	1.0437	0.9898	1.0218	1.0153
345.075	1.0327	1.0120	1.0348	1.0047	1.0265	1.0221
347.750	1.0336	1.0120	0.9920	1.0028	0.9943	1.0069
350.425	1.0248	1.0324	1.0098	0.9888	1.0303	1.0172
353.100	1.0106	1.0129	0.9295	1.0009	1.0274	0.9963
355.775	1.0106	1.0065	0.9732	0.9935	1.0085	0.9985
358.450	1.0239	1.0389	1.0071	1.0651	0.9763	1.0223

IV-B. PROCESSED DATA

Estimation of Average Fracture Aperture from Uranine Elution Profiles

The primary purpose of the uranine experiment was to calibrate the longitudinal dispersivity. However, it was also used to estimate the average value for the fracture aperture. These values were used in the cesium migration experiment simulation described in Section IX-B. Given N outlet sampling points, the procedure given below was used to determine the average fracture aperture, $2b_a$.

Assume that the total fracture volume, V_t, is subdivided into N subvolumes, V_i, of equal width, W/N, and carrying equal flow rates, Q/N, the following equations then relate the aperture in each zone, $2b_i$, to the travel time, t_i, in each zone:

$$L(W/N)2b_i/t_i = Q/N \qquad i = 1,N \qquad \text{(IV-1a)}$$

or

$$2b_i = (Q/LW)\ t_i \qquad i = 1,N \qquad \text{(IV-1b)}$$

therefore,

$$2b_* = (Q/LW)\ t_* \qquad \text{(IV-2)}$$

where "*" denotes the arithmetic mean value.

Also,

$$V_i = L(W/N)\ 2b_i \qquad i = 1,N \qquad \text{(IV-3)}$$

$$V_t = \Sigma\,(V_i) \qquad i = 1,N \qquad \text{(IV-4)}$$

and

$$2b_* = V_t/(LW) \qquad \text{(IV-5)}$$

$$u = Q/W2b_* \qquad \text{(IV-6)}$$

Accordingly, first the time, t_i, at which $A/A^\circ = 0.5$ was identified for each breakthrough curve. Then b_i was computed from Equation (IV-1b), V_i from Equation (IV-3), V_t from Equation (IV-4), $2b_*$ from either Equation (IV-2) or (IV-5), and u from Equation (IV-6). In this experiment, the following values are applicable:

L = 91.5 cm
W = 86.5 cm
N = 5
Q = 20 cm^3/h
$2b_i$ = 580, 475, 570, 655, 835 μm for A, B, C, D, E, respectively
V_t = 493 cm^3
$2b_*$ = 623 μm
u = 3.71 cm/h

The values obtained for b_* and u were input to the computer code for this experiment as well as for the one described in Section IX-B.

IV-C. DATA STORAGE

The data are available on a floppy diskette and may be obtained from the INTRAVAL Secretariat.

V. PREVIOUS MODELING

SMOOTH FRACTURE, PARALLEL PLATE EXPERIMENT

Radionuclide migration studies have been carried out primarily in natural, water-bearing fractures. However, some experiments have been carried out in homogeneous granite blocks containing a parallel fracture with smooth, machined surfaces. The primary reasons for this are as follows:

1. The constant, rectangular cross section of the fracture allows a uniform flow field to be set up. This facilitates the modeling of the transport solution, as channeling in the fracture can be avoided.

2. The homogeneity of the fracture surfaces removes the uncertainty associated with the alteration minerals that coat the surfaces of a natural fracture. Thus, sorption coefficients determined on representative machined granite surfaces are directly applicable to the modeling of the contaminant transport.

The migration experiment was carried out using a 50x10x10 cm granite block with a parallel, polished fracture. The granite was obtained from a commercial granite quarry at the southeastern edge of the Lac du Bonnet batholith, approximately 13 km to the southwest of the town of Lac du Bonnet in Manitoba, Canada. The granite is of the same type as that of the large block and was described in Section I-F.1 (Tammemagi et al., 1980).

As part of the past subsidiary agreement between AECL and DOE, AECL provided to Battelle/OWTD the results of this radionuclide migration experiment which was carried out in a parallel, polished fracture. The details of the experimental setup and corresponding mathematical simulation using FRACFLO are described in Noronha et al., 1988.

VI. EXPECTATIONS FROM INTRAVAL PARTICIPATION

VI-A. EXPERIMENTALIST'S VIEW

These experiments have the unique advantage of having been performed in a natural fracture at a scale of 1 m under controlled, laboratory conditions. Experiments using nonadsorbing tracers such as uranine are potentially useful to estimate the effects of "channeling" on hydrodynamic (longitudinal and transverse) dispersion.

The results from this experiment include the elution profiles of a nonsorbing, or conservative tracer, I-131, and static sorption data on Cs-137 on altered fracture surfaces identical to those used in the migration experiment. Together, the data should be adequate to predict the elution profiles of the Cs-137 from the fracture.

VI-B. MODELER'S VIEW

Most computer codes should be capable of handling the simple geometric design of the experimental setup and flow conditions. The adsorption migration experiment using Cs-137 is valuable to validate mathematical models using experimentally determined sorption parameters.

VII. INFORMATION EXCHANGE

Modeler

Dr. A. Berge Gureghian
Battelle Office of Waste Technology Development
7000 South Adams Street
Willowbrook, Illinois 60521
USA

Phone: (708) 655-8638

Experimentalist

Dr. T.T. Vandergraaf
Geochemistry & Applied Chemistry Branch
Whiteshell Nuclear Research Establishment
Atomic Energy of Canada Limited
Pinawa, Manitoba, Canada ROE 1L0

Phone: (204) 753-2311 Ext. 2592

VIII. POSSIBILITIES FOR FUTURE EXPERIMENTS AND DATA COLLECTION

If it is deemed necessary, the experiments carried out in this effort could be enhanced and improved perhaps with other similar granite blocks that have not been used before. Future experiments could include the determination of tracer concentrations on the fracture surface and in the rock matrix to better validate the sorption aspects of this experiment. In addition, the actual topography of the fracture could be determined to evaluate the flow and transport aspects of channelling within the fracture.

IX. OUTPUT FORMAT

A description of the governing equations used in the mathematical formulation of the FRACFLO code is provided in Appendix A.

IX-A. MATHEMATICAL CALIBRATION OF URANINE EXPERIMENT

As indicated previously, the purpose of this experiment has been to estimate the average fracture aperture and velocity as outlined in Section IV-B and to then calibrate the longitudinal dispersivity (a_L) to achieve close agreement with the elution profiles shown in Figure IV-1. The first step was to interpolate and then arithmetically average the five plots shown in Figure IV-1 into a single "averaged breakthrough curve."

The next step was to run the transport code with the foregoing input parameters and to calibrate a_L until a good match was obtained. The following key input parameters yielded the best match:

Fracture length (L) (Section II-B)	=	91.5 cm
Fracture width (W) (Code requirement: Infinity for 1-D flow field)	=	86.5 cm
Block half-thickness (H) (Code used: Infinite in z-direction)	=	24.5 cm
Fracture volume (V_f) (Section IV-B)	=	493 cm^3
Average fracture aperture ($2b_o$) (Section IV-B)	=	6.23×10^{-2} cm
Volumetric flow rate (Q) (Section IV-A)	=	20 mL/h
Fluid fracture velocity ($u = Q/W2b_o = L/t_T$)	=	3.71 cm/h
Fluid residence (travel) time ($t_T = V_f/Q = L/u$)	=	24.65 h
Half-life of uranine ($T_{\frac{1}{2}}$)	=	∞
Rock density (ρ_r) (Section I-F.2.2)	=	2.65 g/cm^3
Rock porosity (ϕ) (Section I-F.2.2)	=	2×10^{-3}
Pore diffusivity (D_p) (see below)	=	0.0 cm^2/h
Rock adsorption coefficient (K_r)	=	0.0 mL/g
Rock retardation (R')	=	1.0

Fracture surface sorption coefficient (K_f)	=	0.0 cm
Fracture retardation (R)	=	1.0
Longitudinal dispersivity (a_L)	=	3 cm

The agreement between the simulated and experimental results is shown in Figure IX-1. Therefore, this simulation serves to determine that the longitudinal dispersivity, a_L, for LB-2 in its prevailing configuration is 3 cm.

An explanation for the value of pore diffusivity, D_p, used is necessary. It was originally intended that this experiment be performed at a flow rate and velocity high enough that the convection would be so predominant as to completely eclipse the effects of the prevailing matrix diffusion (Section I-E.1.1). In other words, the breakthrough curve at the fracture outlet predicted by the computer code would show no difference as the value of D_p was increased from zero up to the actual value that is appropriate for this tracer/rock combination. So far the value of D_p has not been calibrated. However, it is known that at a flow rate of 20 mL/h, advection completely dominates diffusion. Therefore, D_p can be set equal to zero and expected to obtain the same breakthrough results as if D_p had been assigned its actual value. Figure IX-1 corresponds to the case where D_p is set equal to zero.

The value of $D_p = 1.8 \times 10^{-4}$ cm^2/h derived from the recent literature (Section I-F.2.3) was found to be appropriate for uranine in this granite block. This value has been verified and confirmed in the matrix diffusion simulation described in Section 6.3 of Noronha et al. (1988). To prove the argument made in the last paragraph, Figure IX-2 presents the result of using the actual value for D_p. The breakthrough curve obtained is almost identical to that shown in Figure IX-1.

Finally, Figure IX-3 shows the predicted normalized concentration profiles within the rock matrix corresponding to Figure IX-2. These are calculated at t = 60 hours (2.5 days), which marks the completion of this experiment. Profiles are shown along the centerline of the fracture near the inlet (x = 1 cm), half-way (x = 45 cm), and near the outlet (x = 90 cm). Measurable concentrations are predicted up to about 4 mm away from the fracture wall.

IX-B. MATHEMATICAL CALIBRATION OF THE CESIUM MIGRATION EXPERIMENT

The aim of this experiment was to use the same longitudinal dispersivity, a_L, calibrated in Section IX-A, the diffusivity, D_p, from Table I-3, and the surface sorption coefficient, K_f, from Section IV-A.2 to predict a breakthrough curve for cesium and compare it with the elution profiles shown in Figure IV-2. As before, the first step was to arithmetically average the five plots shown in Figure IV-2 into a single experimental breakthrough curve and to then renormalize the results by multiplying by $e^{-\lambda t}$. This last step is insignificant because $T_{\frac{1}{2}} = 30$ years is so much longer than the approximately 15-day duration of this experiment.

The next step was to run the computer code and to use the input parameters given below to predict a breakthrough curve for cesium.

Fracture length (L) (Section II-B)	=	91.5 cm
Fracture width (W) (Code requirement: Infinity for 1-D flow field)	=	86.5 cm

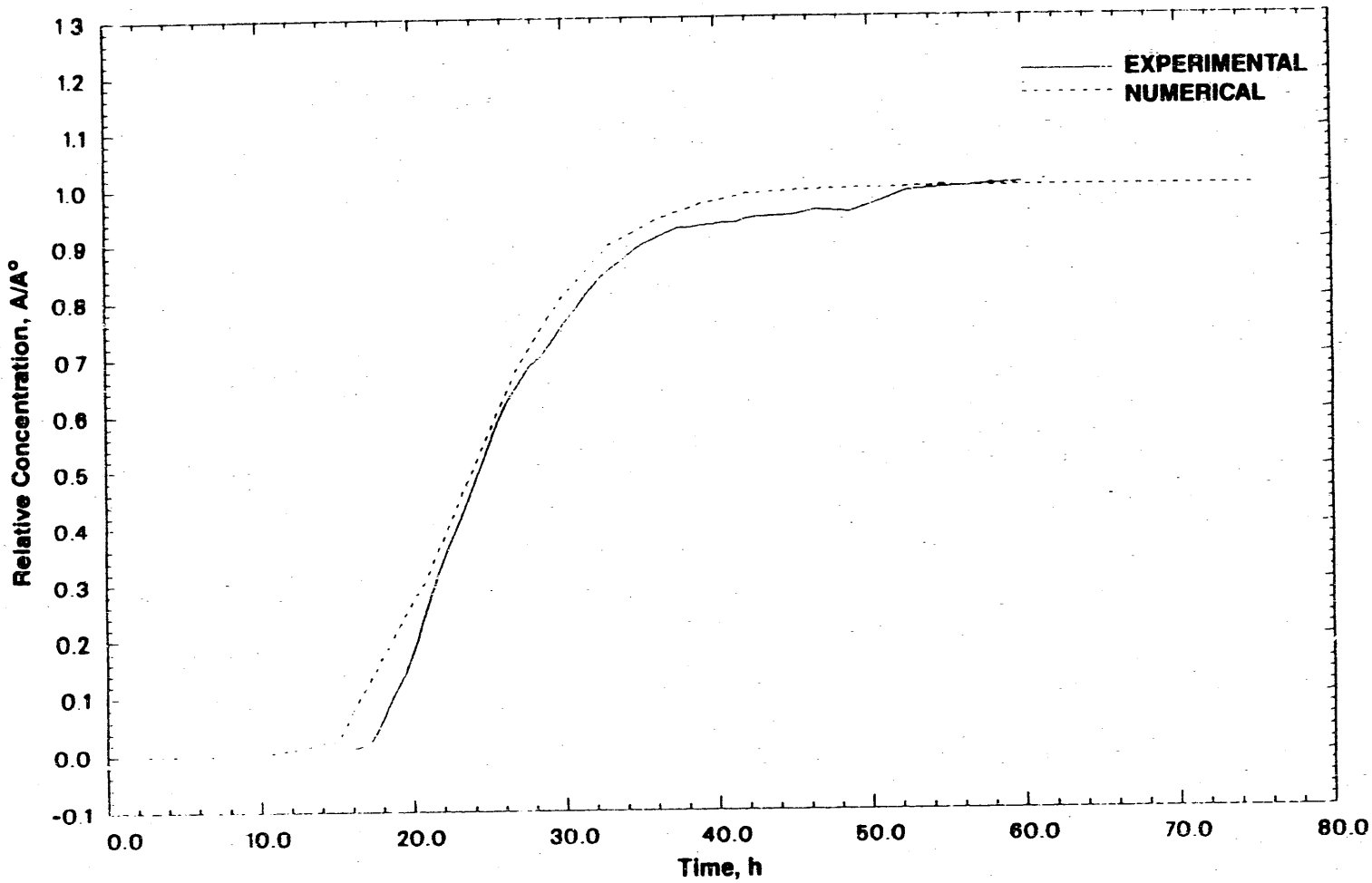

Figure IX-1. Calibration of the Longitudinal Dispersivity a_L, in LB-2 Using the Uranine Breakthrough Curve Versus Time ($D_p = 0.0\ cm^2/h$)

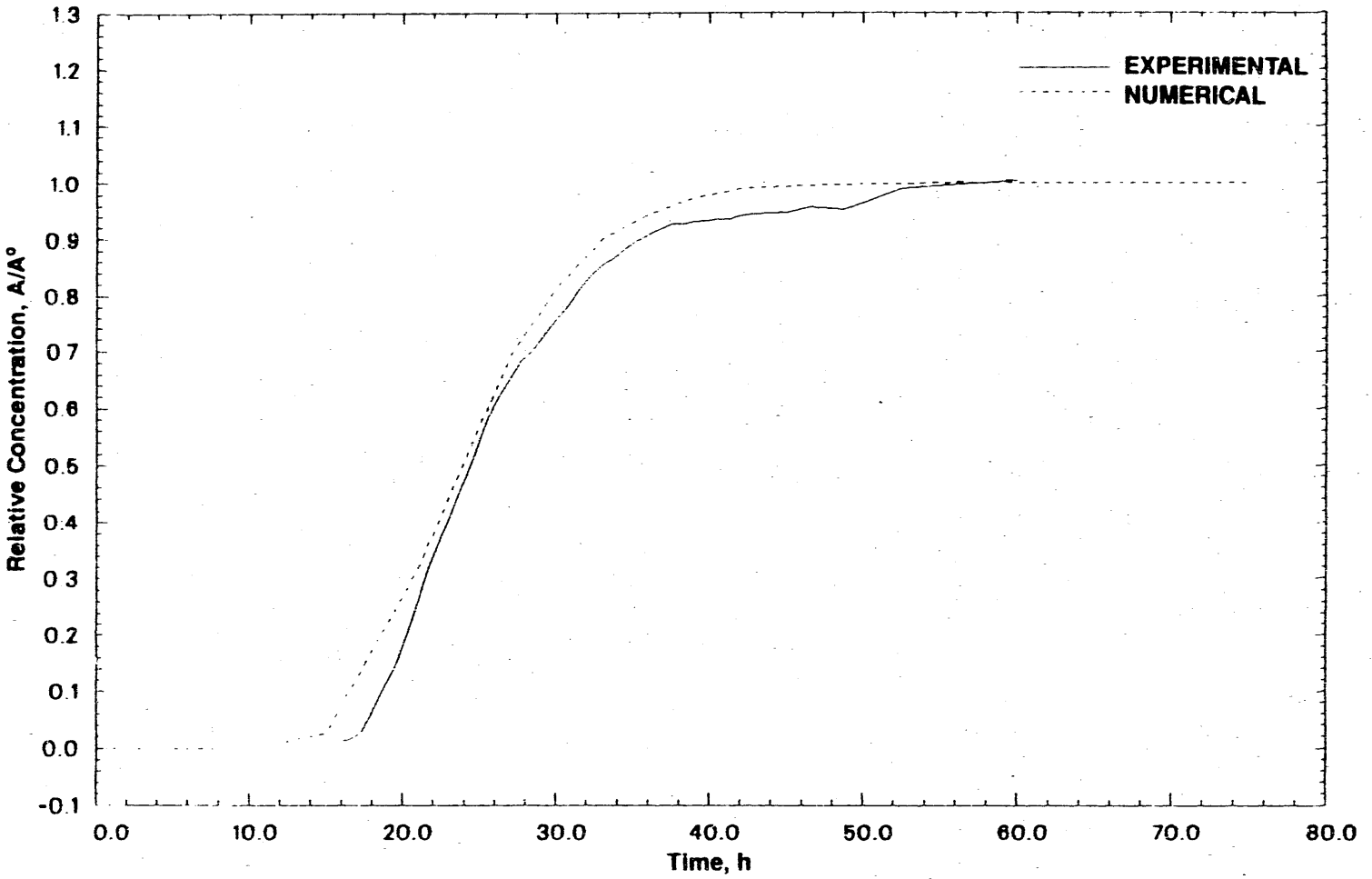

Figure IX-2. Uranine Breakthrough at Fracture Outlet Using Actual Matrix Diffusion ($D_p = 1.8 \times 10^{-4}$ cm^2/h)

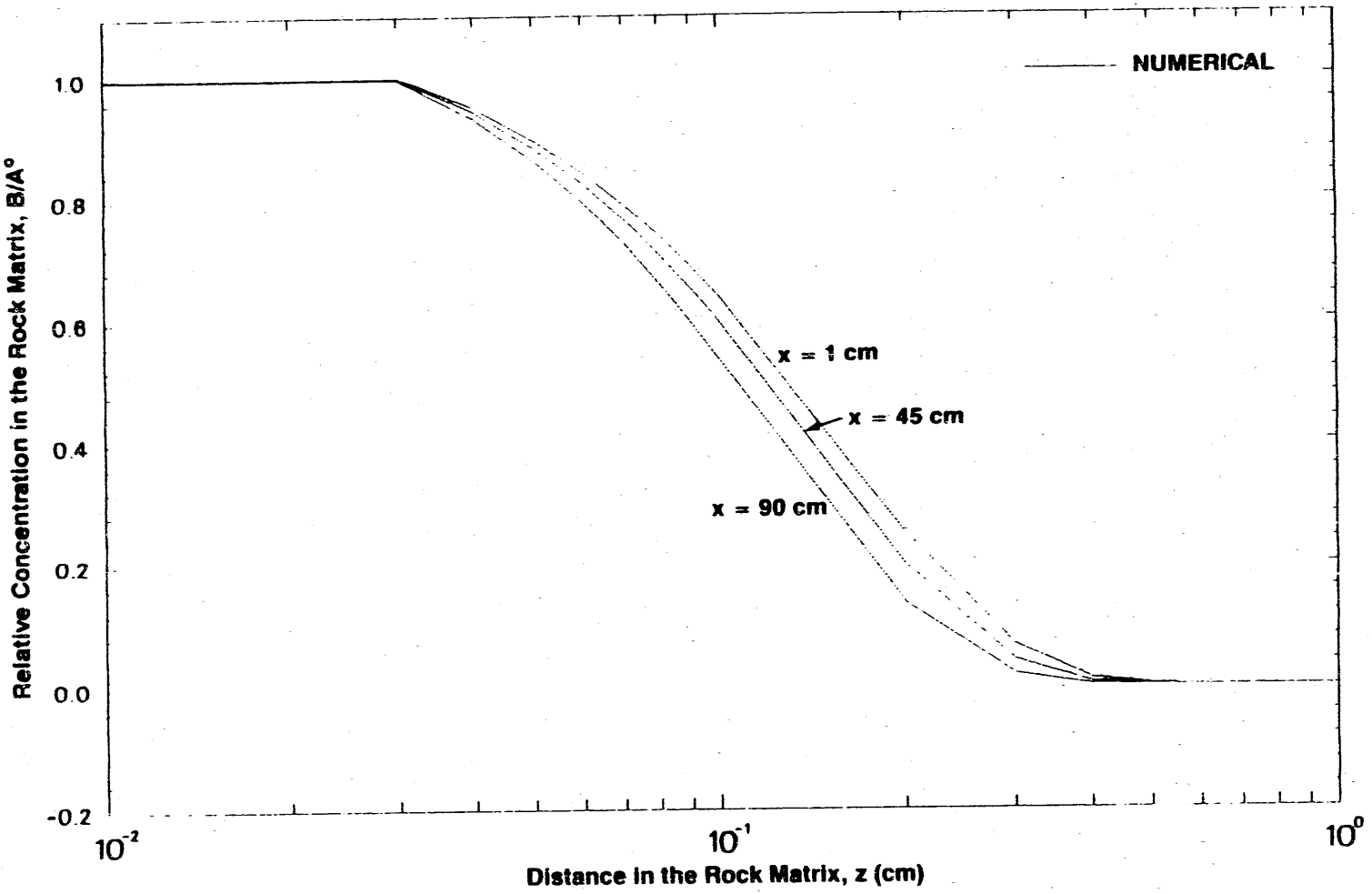

Figure IX-3. Rock Concentration Profiles as a Function of Distance Away From the Fracture for Uranine at the End of the Migration Experiment (t = 2.5 days)

Block half-thickness (H) (Code used: Infinite in z-direction)	=	24.5 cm
Fracture volume (V_t) (Section IV-B)	=	493 cm^3
Average fracture aperture ($2b_o$) (Section IV-B)	=	6.23×10^{-2} cm
Volumetric flow rate (Q) (Section IV-A)	=	20 mL/h
Fluid fracture velocity ($u = Q/W2b_o = L/t_T$)	=	3.71 cm/h
Fluid residence (travel) time ($t_T = V_t/Q = L/u$)	=	24.65 h
Half-life of Cs-137 ($T_{\frac{1}{2}}$)	=	2.63×10^5 h
Rock density (ρ_r) (Section IX-A)	=	2.65 g/cm^3
Rock porosity (ϕ) (Section I-F.2.2)	=	2×10^{-3}
Pore diffusivity (D_p) (Table I-3)	=	1.8×10^{-3} cm^2/h
Longitudinal dispersivity (a_L) (Section IX-A)	=	3 cm
Rock adsorption coefficient (K_r) (Section I-F.3.2)	=	0.34 mL/g
Rock retardation (R')	=	451
Fracture surface sorption coefficient (K_f) (Section IV-A.2)	=	0.06 cm
Fracture retardation (R)	=	2.93

The comparison between the simulated and experimental results is shown in Figure IX-4. Therefore, this experiment validates the use of $K_f = 0.06$ cm for cesium in LB-2.

Note that because of the short time frame of the experiments reported here which never exceeded 15 days, the molecular diffusion effects (see Equation A-5) within the fracture were considered negligible relative to the dispersion effects, hence neglected in the course of the validation effort.

Finally, Figure IX-5 shows the predicted normalized concentration profiles within the rock matrix corresponding to Figure IX-4. These were calculated at t = 360 hours (15 days), which marks the completion of this experiment. Profiles are shown along the centerline of the fracture near the inlet (x = 1 cm), half-way (x = 45 cm), and near the outlet (x = 90 cm). Measureable concentrations were predicted up to only about 2 mm away from the fracture wall. In spite of the order-of-magnitude higher value of D_p used for cesium than uranine, the rock concentrations as well as the penetration of cesium are less than uranine due to retardation resulting from sorption processes. This can be confirmed by superimposing Figures IX-3 and IX-5.

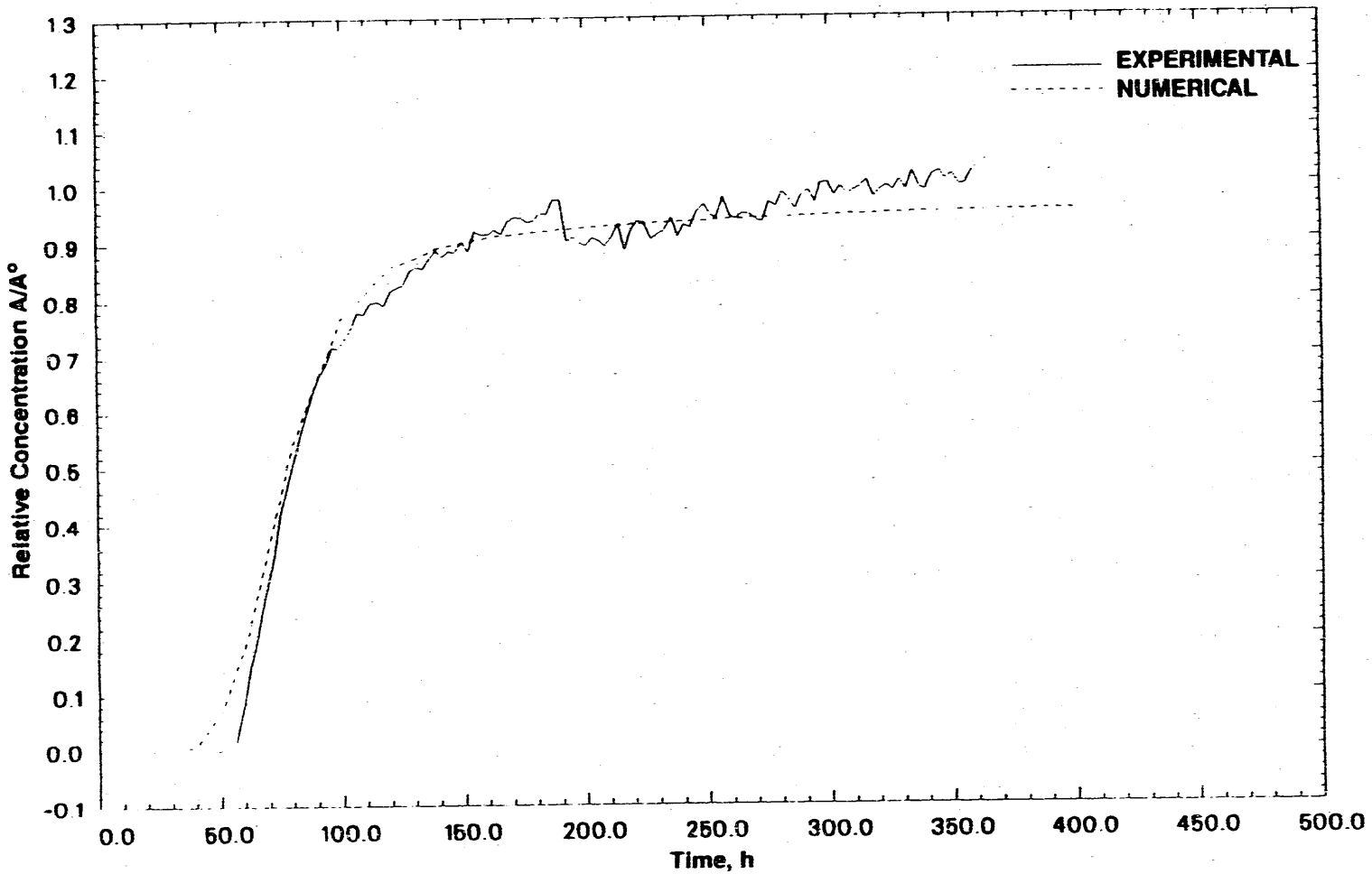

Figure IX-4. Validation of FRACFLO Code Using Experimental Retardation Factors and Cs-137 Breakthrough Curve Versus Time

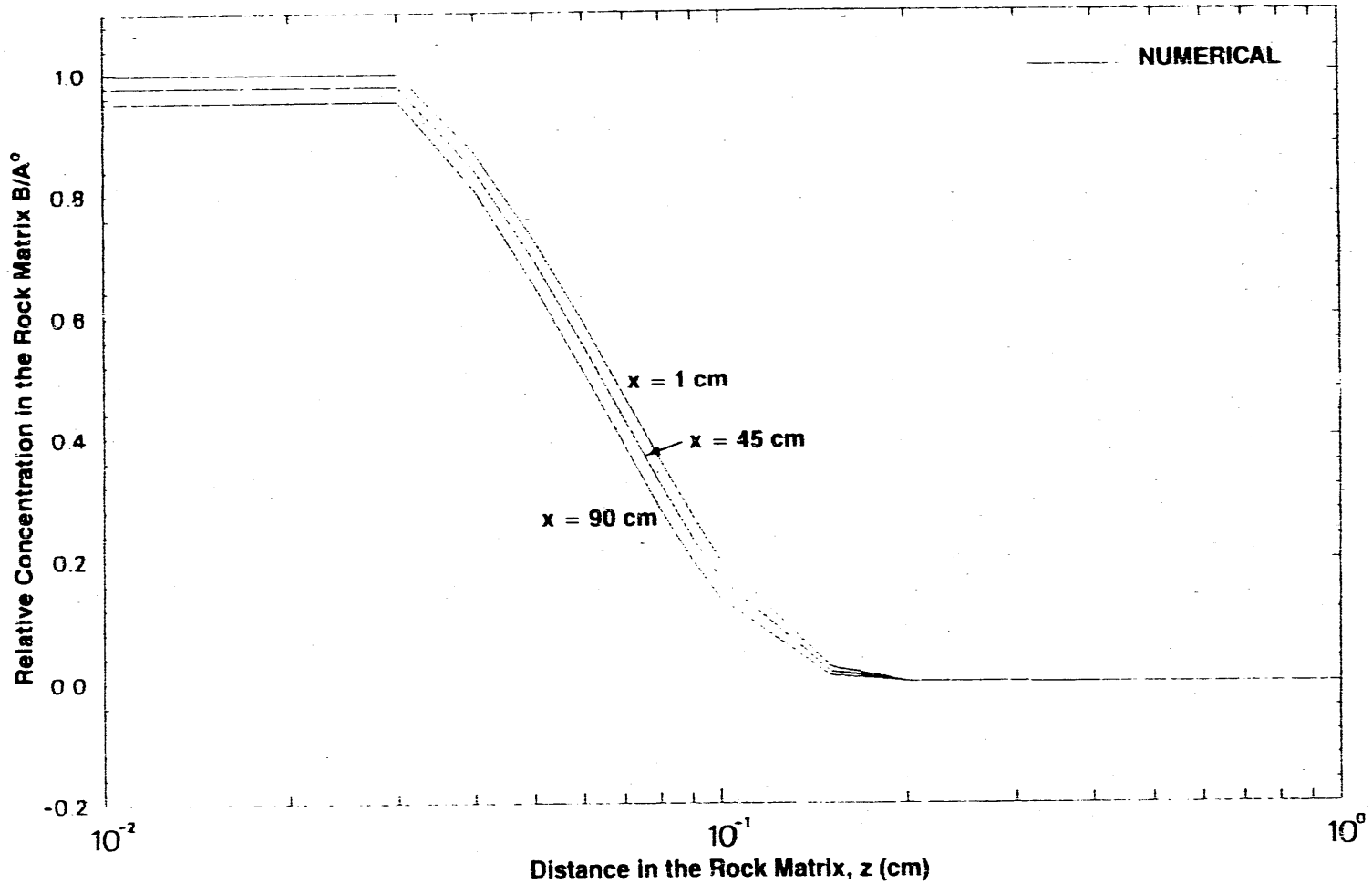

Figure IX-5. Rock Concentration Profiles as a Function of Distance Away From the Fracture for Cs-137 at the End of the Migration Experiment (t = 15 days)

IX-C. OUTPUT FORMAT

The model simulation report submitted to the INTRAVAL Secretariat should contain the following:

- Description of the conceptual model applied
- Mathematical formulation of the model
- Description of how the experimental data have been used for model validation
- Fitting procedure including the goodness-of-fit measure used to match the model results with the experimental data and the free parameters used in the fitting
- Simulation results including the fit between the model results and experimental data, parameter values for the best fit, and views of sensitivity of the fit to variations in different model parameters
- Evaluation of the validity of the model
- Suggestion for improvement of the database and validation procedures.

In addition the Pilot Group may decide that some results should be submitted to the INTRAVAL Secretariat on magnetic tapes in order to facilitate the compilation of the technical reports.

X. REFERENCES

Abry, D.R.M., K. V. Ticknor, and T. T. Vandergraaf, 1982. Procedure to Determine Sorption Coefficients of Radionuclides on Rock Coupons under Static Conditions, Technical Record TR-189, Atomic Energy of Canada Limited, Pinawa, Manitoba.

Ahn, J., P. L. Chambre, and T. H. Pigford, 1986. Radionuclide Migration Through Fractured Rocks: Effects of Multiple Fractures and Two-Member Decay Chains, LBL-21121, Earth Sciences Division, Lawrence Berkeley Laboratory and Department of Nuclear Engineering, University of California, Berkeley, CA.

Bradbury, M. H., D. Lever, and D. Kinsey, 1982. "Aqueous Phase Diffusion in Crystalline Rock," Scientific Basis for Radioactive Waste Management - V, Elsevier Science Publishing Co., Werner Lutze, Editor, pp. 569-578.

Freeze, A. R., and J. A. Cherry, 1979. Groundwater, Prentice-Hall, Inc., Englewood Cliffs, NJ.

Grisak, G. E., and J. F. Pickens, 1980. "Solute Transport Through Fractured Media 2. Column Study of Fractured Till," Water Resources Research, Vol. 16, No. 4, pp., 731-739.

Gureghian, A. B., 1990. FRACFLO: Analytical Solutions for Two-Dimensional Transport of a Decaying Species in a Discrete Planar Fracture and Equidistant Multiple Parallel Fractures With Rock Matrix Diffusion, BMI/OWTD-5, Office of Waste Technology Development, Battelle, Willowbrook, IL,.

Huyakorn, P.S., B. H. Lester, and J. W. Mercer, 1983. "An Efficient Finite Element Technique for Modeling Transport in Fractured Porous Media 1. Single Species Transport", Water Resources Research, Vol. 19, No. 3, pp. 841-854.

Lallemand-Barres, A., and P. Peaudecerf, 1978. "Recherches des relations entre la valeur de la dispersivité macroscopique d'un milieu aquifère, ses autres characteristiques et les conditions de mesure," Bull. Bur. Rech. Geol. Min., Sect. 3, Ser. 2, No. 4, pp. 277-284.

Melnyk, T. W., and A.M.M. Skeet, 1986. "An Improved Technique for the Determination of Rock Porosity," Canadian Journal of Earth Sciences, Vol. 23, pp. 1068-1074.

Neretnieks, I., 1980. "Diffusion in the Rock Matrix: An Important Factor in Radionuclide Retardation?" Journal of Geophysical Research, Vol. 85, No. B8, pp. 4379-4397.

Noorishad, J., and M. Mehran, 1982. "An Upstream Finite Element Method for Solution of Transient Transport Equations in Fractured Porous Media," Water Resources Research, Vol. 18, No. 3, pp. 588-596.

Noronha, C. J., J. E. Byrd, and A. B. Gureghian, 1988. "Calibration and Validation of the FRACFLO Code Using the Large Block Migration Experiments," Internal Technical Memorandum, W/TM-1, Office of Waste Technology Development, Battelle Project Management Division, Willowbrook, IL.*

*Available by request from the project files.

Novakowski, K. S., G. V. Evans, D. A. Lever, and K. G. Raven, 1985. "A Field Example of Measuring Hydrodynamic Dispersion in a Single Fracture," Water Resources Research, Vol. 21, No. 8, pp. 1165-1174.

Ogata, A., and R. B. Banks, 1961. "A Solution of the Differential Equation of Longitudinal Dispersion in Porous Media," Fluid Movement in Earth Materials, Geological Survey Professional Paper 411-A, U.S. Government Printing Office, Washington, D.C.

Rasmuson, A., and I. Neretnieks, 1981. "Migration of Radionuclides in Fissured Rocks: The Influence of Micropore Diffusion and Longitudinal Dispersion," Journal of Geophysical Research, Vol. 86, No. B5, pp. 3749-3758.

Skagius, K., and I. Neretnieks, 1988. "Measurements of Cesium and Strontium Diffusion in Biotite Gneiss," Water Resources Research, Vol. 24, No. 1, pp. 75-84.

Sudicky, E. A., and E. O. Frind, 1982. "Contaminant Transport in Fractured Porous Media: Analytical Solutions for a System of Parallel Fractures," Water Resources Research, Vol. 18, No. 6, pp. 1634-1642.

Tammemagi, H. Y., P. S. Kerford, J. C. Requelma, and C. A. Temple, 1980. A Geological Reconnaissance Study of the Lac du Bonnet Batholith, Atomic Energy of Canada Limited Report, AECL-6439, Pinawa, Manitoba.

Tang, D. H., E. O. Frind, and E. A. Sudicky, 1981. "Contaminant Transport in Fractured Porous Media: Analytical Solution for a Single Fracture," Water Resources Research, Vol. 17, No. 3, pp. 555-564.

Ticknor, K. V. (unpublished results)*

Vandergraaf, T. T., D.R.M. Abry, and C. E. Davis, 1982. "The Use of Autoradiography in Determining the Distribution of Radionuclides Sorbed on Thin Sections of Plutonic Rocks from the Canadian Shield," Chemical Geology, Vol. 36, pp. 135-154.

Vandergraaf, T. T., D. M. Grondin, P. Vilks, and D. J. Drew, 1986. Second International Conference on Radioactive Waste Management, Canadian Nuclear Society, pp. 142-150.

*Available by request from the project files.

APPENDIX A

MASS TRANSPORT EQUATIONS FOR FRACTURE AND ROCK MATRIX

The mass transport equations presented in this appendix represent the governing one-dimensional equations describing the migration process of a radionuclide in an idealized fractured rock system based on the discrete fracture approach. The boundary conditions, as well as the type of release modes associated with the migration process which are handled by the analytical solutions presented in FRACFLO (see Gureghian, 1990), are also reported.

A.1 GOVERNING EQUATIONS

From the mass conservation requirement, the equations describing the concentration of a nuclide flowing in a discrete fracture plane with uniform aperture while undergoing sorption and infinite diffusion in the surrounding rock matrix under isothermal and laminar flow conditions are given by

(a) Fracture

$$R \frac{\partial A}{\partial t} - D_x \frac{\partial^2 A}{\partial x^2} + u \frac{\partial A}{\partial x} + \lambda R A + \frac{J}{b} = 0 \qquad (A\text{-}1)$$

(b) Rock Matrix

$$R' \frac{\partial B}{\partial t} - D_p \frac{\partial^2 B}{\partial z^2} + \lambda R' B = 0 \qquad (A\text{-}2)$$

where

A is the concentration in the fracture (ML^{-3})

R is the retardation factor in the fracture

D_x is the hydrodynamic dispersion coefficient in the x direction of the fracture (L^2T^{-1})

u is the average fluid velocity in the fracture (LT^{-1})

λ is the first-order rate constant for decay (T^{-1})

J is the diffusive rate of nuclide at surface of fracture per unit area of fracture surface ($ML^{-2}T^{-1}$)

b is the half-thickness of the fracture (L)

R' is the retardation factor in the rock matrix

B is the concentration in the rock matrix (ML^{-3})

D_p is the pore diffusivity (L^2T^{-1})

t is the time (T).

The diffusive rate of a nuclide into the rock matrix is assumed to obey Fick's law of diffusion written as

$$J = - D_e \frac{\partial B}{\partial z} \Big|_{z=b} \qquad (A\text{-}3)$$

where D_e is the effective diffusivity in the rock matrix (Neretnieks, 1980) defined as

$$D_e = \phi D_p \qquad (A\text{-}4a)$$

and

$$D_p = D_d g_f \qquad (A\text{-}4b)$$

where

ϕ is the rock porosity

D_d is the molecular diffusion of nuclide in water (L^2T^{-1})

g_f is the geometric factor i.e. $\frac{\delta_d}{\iota^2}$ where

δ_d is the constrictivity for diffusion (L^0)

ι is the tortuosity of the rock matrix (L^0).

The hydrodynamic dispersion in the fracture (Bear, 1972) is given by

$$D_x = a_L u + \iota D_d \qquad (A\text{-}5)$$

where

a_L is the longitudinal dispersivity (L)

ι is the tortuosity of the fracture (L^0)

The retardation factor in the fracture and rock matrix: R and R' (Neretnieks et al., 1982) are given by:

$$R = 1 + K_f/b \qquad (A\text{-}6a)$$

$$R' = 1 + [(1 - \phi)/\phi]\rho_r K_r \qquad (A\text{-}6b)$$

where

ρ_r is the rock density (ML^{-3})

K_f is the surface distribution coefficient in the fracture (L)

K_r is the distribution coefficient in the rock matrix (L^3M^{-1}).

A.2 INITIAL AND BOUNDARY CONDITIONS

The set of differential equations, Equations A-1 and A-2, are subject to the initial conditions:

$$A(x,0) = 0, 0 < x < \infty \tag{A-7}$$

$$B(x,z,0) = 0\ ,\ x > 0\ ,\ z \geq b \tag{A-8}$$

and boundary conditions in the fracture and rock matrix. The boundary conditions in the fracture are given by

$$A(0,t) = A(t)\,U(t), t > 0 \tag{A-9a}$$

$$A(\infty,t) = 0\ ,\ t > 0 \tag{A-9b}$$

where

$A(t)$ is the concentration at the source.

In the rock matrix, the boundary conditions are:

$$B(x,b,t) = A(x,t)\ ,\ x > 0 \tag{A-10a}$$

$$B(x,\infty,t) = 0\ ,\ t > 0 \tag{A-10b}$$

For a step release mode (continuous decaying source), the concentration at the source for a typical nuclide may be written as

$$A(t) = A^0 e^{-\lambda t} \tag{A-11}$$

where

A^0 is the concentration of the species at time equals zero.

For a band release mode, the boundary condition for the band release may be written as

$$A(0,y,t) = A(t)[U(t) - U(t-T)]\ ,\ t > 0 \tag{A-12}$$

where

T is the leaching time.

U(t−T) is the Heaviside unit function defined as

$$U(t-T) = \begin{cases} 1, t \geq T \\ 0, t < T \end{cases} \quad \text{(A-13)}$$

The general form of the solution for the band release mode based on a boundary condition given by Equation A-12 and which uses the superposition technique (see Foglia et al., 1979) may be written as

$$^{b}A(x,y,t) = [A(x,t; A^{0}) - A(x,t-T; A^{0}e^{-\lambda T})]U(t-T) \quad \text{(A-14)}$$

A.3 REFERENCES

Bear, J., 1972. Dynamics of Fluid in Porous Media, American Elsevier Publishing Co., New York, NY.

Foglia, M., F. Iwamoto, M. Harada, P. L. Chambre, and T. H. Pigford, 1979. "The Superposition Equation for the Band Release of Decaying Radionuclides Through Sorbing Media," UCB-NE-3335, University of California at Berkeley, ANS Transactions, Volume 33, pp. 384-386.

Gureghian, A. B., 1990. FRACFLO: Analytical Solutions for Two-Dimensional Transport of a Decaying Species in a Discrete Planar Fracture and Equidistant Multiple Parallel Fractures With Rock Matrix Diffusion, BMI/OWTD-5, Office of Waste Technology Development, Battelle, Willowbrook, IL.

Neretnieks, I., 1980. "Diffusion in the Rock Matrix : An Important Factor in Radionuclide Retardation?" Journal of Geophysical Research, Vol. 85, pp. 4379-4397.

Neretnieks, I., T. Eriksen, and P. Tahtinen, 1982. "Tracer Movement in a Single Fissure in Granitic Rock: Some Experimental Results and Their Interpretation," Water Resources Research, Vol. 18, No. 4, pp. 849-858.

APPENDIX B

NOTATIONS

Terms

a_l	longitudinal dispersivity
A	concentration in the fracture
A^0	concentration of the species at the source at time equals zero
b	half-thickness of the fracture
$2b_t$	average fracture aperture (arithmetic mean value)
B	concentration in the rock matrix
D_d	molecular diffusion of nuclide in water
D_e	effective diffusivity in the rock matrix
D_p	pore diffusivity
D_x	hydrodynamic dispersion coefficient in the fracture
g_f	geometric factor $(\delta_d/_t'^2)$
H	block half thickness
K_f	surface distribution coefficient in the fracture
K_r	distribution coefficient in the rock matrix
L	fracture length
N	number of subvolume
Q	volumetric flow rate
R	retardation factor in the fracture
R'	retardation factor in the rock matrix
t	time
t_T	fluid residence (travel) time
T	leaching time
$T_{\frac{1}{2}}$	half-life
u	average fluid velocity in the fracture

V_t	fracture volume
W	fracture width
x	position vector in the fracture
z	position vector in the rock matrix
δ_d	constrictivity for diffusion
λ	first-order rate constant for decay
ρ_r	rock density
τ	tortuosity of the fracture
τ'	tortuosity of the rock matrix
ϕ	rock porosity

END

DATE FILMED

11 / 08 / 90